TRPγ regulates lipid metabolism through *Dh44* neuroendocrine cells

Dharmendra Kumar Nath[1,#], Subash Dhakal[1,#], and Youngseok Lee[1*]

[1]Department of Bio and Fermentation Convergence Technology, Kookmin University, Seoul, 02707, Republic of Korea

[#] These authors contributed equally to this work

*Correspondence and requests for materials should be addressed to:

Y.L. (email: ylee@kookmin.ac.kr; ORCID: 0000 0003 0459 1138)

ABSTRACT

Understanding how the brain controls nutrient storage is pivotal. Transient receptor potential (TRP) channels are conserved from insects to humans. They serve in detecting environmental shifts and in acting as internal sensors. Here, we found that a TRPγ mutant exhibited in *Drosophila melanogaster* are required for maintaining normal lipid and protein levels. In animals, lipogenesis and lipolysis control lipid levels in response to food availability. Lipids are mostly stored as triacylglycerol in the fat bodies (FBs) of *D. melanogaster*. Interestingly, *trpγ* deficient mutants exhibited elevated TAG levels and our genetic data indicated that *Dh44* neurons are indispensable for normal lipid storage but not protein storage. The *trpγ* mutants also exhibited reduced starvation resistance, which was attributed to insufficient lipolysis in the FBs. This could be mitigated by administering lipase or metformin orally, indicating a potential treatment pathway. Gene expression analysis indicated that *trpγ* knockout downregulated *brummer*, a key lipolytic gene, resulting in chronic lipolytic deficits in the gut and other fat tissues. The study also highlighted the role of specific proteins, including neuropeptide DH44 and its receptor DH44R2 in lipid regulation. Our findings provide insight into the broader question of how the brain and gut regulates nutrient storage.

Keywords: TRP channel, Dh44, metabolism, lipid

INTRODUCTION

Nutrient storage is not a simple matter of accumulation but involves a sophisticated network of signals and receptors, feedback loops, and hormonal influences, all choreographed by the brain. The mechanisms involve various tissues and organs, including the liver, muscles, and adipose tissue, each playing a distinct role in the storage and release of vital nutrients like glucose, fats, and proteins in mammals (Efeyan et al., 2015). Key to this regulation are specialized cells and molecular pathways that respond to dietary intake, energy expenditure, and changes in the internal and external environment (Tran et al., 2022). For instance, the brain receives and interprets signals about the body's energy status through hormones such as insulin and leptin, and nutrients themselves, which inform decisions on whether to store or mobilize energy reserves in mammals (Jais and Brüning, 2022; Roh and Kim, 2016). Moreover, the role of Transient Receptor Potential (TRP) channels as molecular sensors that detect changes in the environment and internal metabolic status highlights the level of molecular sophistication involved in nutrient storage and energy balance (Clapham, 2003; Dhakal and Lee, 2019; Fowler and Montell, 2013; Turner et al., 2016). These channels bridge external stimuli with internal responses, ensuring the body adapts efficiently to maintain homeostasis (Dhakal and Lee, 2019; Venkatachalam and Montell, 2007). This concert of mechanisms, from the molecular to the systemic level, exemplifies the elegance with which the brain ensures our energy needs are met in a changing environment, highlighting the intricate interplay of biological process that sustains life (Picard et al., 2018). Understanding these processes opens up new vistas in our approach to diet, disease management, and overall health optimization.

The use of a genetically tractable model organism such as *Drosophila melanogaster* could provide fundamental insights into the potential relationship between TRP channels and metabolic syndrome. This study delves into the function of TRPγ channels, specifically their role in managing lipid and protein levels. Through genetic manipulation, we explored the consequences of TRPγ mutations on the metabolic processes, revealing critical insights into the regulation of lipid storage and breakdown. We found that TRPγ expression in *Dh44* neuroendocrine cells in the brain is critical for maintaining normal carbohydrate levels in tissues (Dhakal et al., 2022). Building on this, we hypothesized that TRPγ in *Dh44* cells also regulates lipid and protein homeostasis. Our investigation sheds light on the balance between lipogenesis and lipolysis, processes that respectively synthesize and degrade lipids based on the availability of food, and how these processes are affected by TRPγ activity. By examining the metabolic anomalies in *trpγ* deficient mutants, including alterations in lipid storage and the consequent impact on starvation resistance, this study advances our understanding of metabolic regulation. Furthermore, we uncover the potential therapeutic benefits of lipase and metformin in counteracting the metabolic deficiencies caused by TRPγ mutations. Through detailed gene expression analysis, we identify the downregulation of crucial genes involved in lipid metabolism, offering new perspectives on the genetic underpinnings of nutrient storage regulation. The implications of this research are far-reaching, not only enhancing our comprehension of basic biological functions but also providing avenues for therapeutic interventions in metabolic disorders.

RESULTS

TRPγ mutants exhibit reduced sugar level alongside elevated lipid and protein levels

In order to understand how *D. melanogaster* regulates the maintenance of major nutrient levels, including carbohydrates, lipids, and proteins, TRP channel mutants were examined as potential candidates. A recent study revealed that among TRP channel mutants, only *trpγ* mutant displayed only reduced carbohydrate levels (Dhakal et al., 2022), suggesting the involvement of additional TRP channels in regulating major nutrients. *D. melanogaster* possesses 13 members of the TRP channel family. Flies with mutations in *trpM*, *trpML*, and *nompC* showed high mortality rates with minimal survival, whereas those with mutations in the remaining 10 TRP superfamily genes were viable and healthy when homozygous. Investigation into the lipid and protein levels of other available TRP superfamily mutants under sated condition revealed that, apart from the *trpγ* mutant, all tested mutants exhibited normal levels (***Figure 1A and B***). Specifically, the $trp\gamma^{1}$ mutant showed 1.3 times higher triacylglycerol (TAG) levels and 1.5 times higher protein levels compared to the control. These metabolic changes were unique and specific to the *trpγ* mutants among the evaluated TRP superfamily mutants. Previous observations indicated that *trpγ* mutants had lower cellular sugar levels and stored glycogen (Dhakal et al., 2022). Consistently, *trpγ* mutants exhibited reduced levels of cellular sugars (glucose and trehalose), stored glycogen, and sugar levels in the hemolymph (***Figure 1C–E***). In conclusion, it was found that $trp\gamma^{1}$ mutants displayed lower carbohydrate levels but higher lipid and protein levels compared to the control.

Importantly, the increased TAG and protein levels observed in *trpγ*^{1} mutants were confirmed with a second *trpγ*^{1} allele (*trpγ*^{G4}) (***Figure 1F and G***). Furthermore, we restored the deficiency in lipid and protein levels using a genomic *trpγ*$^{+}$ transgene, *g*(*trpγ*), and by introducing a *UAS-trpγ* cDNA, controlled by *GAL4* knocked into the *trpγ* locus (*trpγ*^{G4} flies; +).

TRPγ regulates lipid metabolism through Dh44 neuroendocrine cells in the pars intercerebralis

We recently proposed that TRPγ expression in the six DH44 neuroendocrine cells in the pars intercerebralis (PI) located in the dorsal medial area of the brain (***Figure 2–figure supplement 1A1–A3***) is essential to maintain normal carbohydrate levels in tissues (Dhakal et al., 2022). Therefore, we next sought to determine whether protein and lipid levels can be regulated by the same neuroendocrine cells. To test this, we used a transgenic fly encoding an inwardly rectifying K^{+} channel (*UAS-Kir2.1*) to inactivate specific neurons (Hodge, 2009). Interestingly, inactivating the *Dh44* neurons significantly increased the lipid levels but not protein levels (***Figure 2A and B***). Approximately 16 neurons in the PI express dILP2, which are also overlapped by two DH44-positive neurons in 5 to 10 days old adult male flies (***Figure 2–figure supplement 1B1–B3***) (Ohhara et al., 2018). However, inactivation of *dILP2* neurons did not impair either lipid or protein levels (***Figure 2A and B***). In conclusion, our findings indicated that DH44 neuroendocrine cells contribute to lipid regulation but not protein regulation.

To assess whether *trpγ* expression in *Dh44* neurons is sufficient to restore normal lipid and protein levels in *trpγ* mutant flies, we expressed the *UAS-trpγ* under the control of *Dh44-GAL4* in the $trp\gamma^{1}$ mutant background (***Figure 2C and D***). Our findings indicated that the increased lipid levels in the $trp\gamma^{1}$ mutant background decreased to normal levels via the expression of the *trpγ* transgene in the DH44 neuroendocrine cells but not in its parent strains (***Figure 2C***). Again, the expression of the *trpγ* transgene in the dILP2 neurons had no appreciable effects (***Figure 2C***). In contrast, the expression of the *trpγ* transgene did not decrease the protein levels in either the DH44 or the dILP2 neurons (***Figure 2D***). This indicates that TRPγ expressed in Dh44 cells is sufficient for the regulation of lipid level. Next, RNAi-mediated knockdown experiments were conducted to further examine the role of *trpγ* in *Dh44* neurons. Interestingly, *trpγ* knockdown in *Dh44* neurons significantly increased lipid levels, whereas flies harboring only the *Dh44-GAL4* or the $UAS\text{-}trp\gamma^{RNAi}$ transgenes displayed normal lipid levels (***Figure 2E***). This indicated that TRPγ in Dh44 cells is needed for the regulation of lipid levels. Furthermore, the total TAG level in the $trp\gamma^{1}$ flies was higher in both males and females (***Figure 2–figure supplement 1C***), meaning that the functions of *trpγ* are not sex-specific.

In *D. melanogaster*, lipids are mainly stored in the form of TAG and cholesterol ester in the adipose tissue [i.e., fat bodies (FBs)] as lipid droplets (LDs) (Liu and Huang, 2013). Consistent with the increased TAG in tissues, Nile red staining of the FBs of $trp\gamma^{1}$ and $trp\gamma^{G4}$ flies exhibited larger lipid mass compared to control animals under sated condition (***Figure 2F–I***). These LDs returned to their normal size through the expression

of *trpγ* in *trpγ* or *Dh44* neurons but not *dILP2* neurons (***Figure 2F and 2J–L***). Additionally, inactivating the *Dh44* cells (*Dh44-GAL4*/*UAS-Kir2.1*) recapitulated the enlarged LD phenotype of the *trpγ* mutant flies (***Figure 2–figure supplement 1D–G***). Overall, our findings indicated that *trpγ* expression regulates lipid and carbohydrate homeostasis but not protein levels in DH44 neuroendocrine cells in the PI.

TRPγ mutants exhibit starvation susceptibility and deficits in lipolysis

Higher lipid cellular levels may decrease lifespan (Johnson and Stolzing, 2019; Tatar et al., 2014). Therefore, we measured the lifespan of control and $trp\gamma^{1}$ flies fed with a standard cornmeal diet (***Figure 3A***). However, the lifespans of control and $trp\gamma^{1}$ flies were not significantly different under normal conditions. The LT_{50} of the control was 59.34 ± 0.92 days and that of $trp\gamma^{1}$ was 55.75 ± 2.35 days. In contrast, *trpγ* appeared to be required for proper metabolism under starvation conditions, as demonstrated by the decreased starvation resistance of the $trp\gamma^{1}$ and $trp\gamma^{RNAi}$ knockdown flies in *Dh44* cells (***Figure 3B***) (Dhakal et al., 2022). This defect was fully recovered by the expression of *UAS-trpγ* under the control of *Dh44-GAL4* (***Figure 3B***).

The starvation sensitive phenotype in the *trpγ* mutants may have been due to decreased carbohydrate storage in tissues, including glucose, trehalose, and glycogen. However, we previously demonstrated that *trpγ* mutants could utilize carbohydrates under starved conditions (Dhakal et al., 2022). Furthermore, the elevated whole-body TAG levels in the *trpγ* mutant flies might suggest that they were unable to break down stored lipids even under starving conditions. Metazoans must coordinate the

metabolism of glycogen, lipid, and protein to maintain metabolic homeostasis during fasting periods, thus providing an appropriate energy supply across tissues. Therefore, the total TAG levels of the control and *trpγ* mutant flies were assessed under sated and starved (starvation for 24 h) conditions (***Figure 3C–F)***. When the control flies were deprived of food for 24 h, their TAG levels decreased significantly (***Figure 3C***). In contrast, the $trp\gamma^{1}$ mutants exhibited no changes in whole-body TAG levels before and after starvation (***Figure 3C***). To further confirm that lipolysis was restricted in the *trpγ* mutants under starvation conditions, LDs were stained, after which we measured the sizes of individual LDs accumulated throughout the whole fat bodies of the flies (***Figure 3D–F***). Despite considerable variations, the sizes of the LDs in the control flies were significantly reduced after starvation. In contrast, no significant differences in LD sizes were identified between the sated and starved conditions in the $trp\gamma^{1}$ flies. We examined how overexpression and knockdown of *trpγ* in *Dh44* neurons affect the starvation phenotype. Overexpressing *trpγ* in *Dh44* cells resulted in similarity to the wild-type in both sated and starved conditions, as well as normal survival time under starvation conditions (***Figure 3B and Figure 3–figure supplement 1A***). Conversely, $trp\gamma^{RNAi}$ knockdown flies in *Dh44* neurons reproduced phenotypic traits observed in *trpγ* mutants, including decreased lipid levels (***Figure 3–figure supplement 1B***) and reduced survival time under starvation conditions (***Figure 3B***).

Dh44 neurons regulate starvation-induced sleep suppression (Oh and Suh, 2023), which implies that these neurons become more active under starved conditions. Adenosine monophosphate-activated protein kinase (AMPK) serves as the master

controller for maintaining energy balance in cells, coordinating metabolic pathways (Hardie et al., 2003). It regulates the balance between building up and breaking down substances to ensure cellular stability during metabolic stress. AMPK is a key target for treating metabolic diseases like type 2 diabetes and obesity, as its activation increases fatty acid oxidation (Kim et al., 2016). We wonder if activating AMPK in *Dh44* neurons improve lipolysis. The expression of $AMPK^{TD}$, activated form of AMPK (Lee et al., 2007) in *Dh44* neurons indeed restored the elevated TAG levels observed in $trp\gamma^{1}$ (***Figure 3G***). This suggests that AMPK functions as a downstream component of *Dh44* neuronal activation.

Recovery of the starvation resistance of the TRPγ mutant via metformin treatment

Metformin is widely used to treat many metabolic diseases such as type II diabetes (Lv and Guo, 2020). We previously demonstrated that 1 to 5 mM metformin can induce hypoglycemia, in addition to suppressing fat storage in flies (Nath and Lee, 2024; Sang et al., 2021). Therefore, we next sought to test whether the increased lipid levels of the *trpγ* mutant can be reduced to a normal level via oral administration of metformin. First, we measured TAG levels at 0, 7, and 14 days after dietary administration of 1 mM or 5 mM of metformin (the treatments were prepared by mixing the appropriate metformin concentrations into standard cornmeal diets) (***Figure 4A and B***). The high TAG levels in the *trpγ* mutant (41.91 ±4.56) were decreased to levels similar to those of the control at 7 and 14 days (30.03 ±4.34 and 33.79 ±3.20, respectively) after treatment with 1 mM metformin (***Figure 4A***). Furthermore, although oral administration of 1 mM metformin did not affect the TAG level in the control, the 5 mM metformin treatment significantly

reduced the TAG level of the control flies at 14 days (***Figure 4B***). Moreover, the 5 mM metformin treatment was more effective in reducing the TAG level in the *trpγ* mutant. These findings indicated that oral administration of metformin can either suppress lipogenesis or enhance lipolysis in *D. melanogaster*. To further confirm the effects of metformin treatment, LDs were analyzed under the same condition (***Figure 4C and D***). The sizes of the LDs in the control and *trpγ* mutant flies were significantly reduced after treatment with 1 mM metformin at 14 days or 5 mM metformin at 7 and 14 days (***Figure 4D***).

Next, we sought to assess whether metformin could increase starvation resistance in the control and *trpγ* mutant flies. To test this hypothesis, the starvation resistance of the flies was measured with or without metformin. Neither of the metformin concentrations appeared to affect the starvation resistance of the control flies (***Figure 4E and F***). However, although metformin did not restore the starvation resistance of the *trpγ* mutant flies to the level of the controls, it did significantly extend their survival (***Figure 4E and F***; LT_{50} of the control at 1 mM and 5 mM: 56.06 ±1.40 h and 52.39 ±2.09 h, respectively; LT_{50} of the $trp\gamma^{1}$ mutant at 1 mM and 5 mM: 50.35 ±3.34 h and 46.42 ±1.54 h, respectively). Our findings thus demonstrated that oral metformin administration can rescue TRPγ-mediated metabolic syndrome.

Downregulation of the lipolytic gene *brummer* in *trpγ* mutants

The $trp\gamma^{1}$ mutants exhibited marked alterations in the levels of major nutrients. Therefore, we next sought to analyze the transcriptional levels of genes related to

gluconeogenesis, lipogenesis, and lipolysis. Gluconeogenesis is a metabolic process that produces glucose from non-carbohydrate carbon substrates. The genome of *D. melanogaster* harbors two gluconeogenic genes: *fructose-1,6-bisphosphatase* (*fbp*) and *phosphoenolpyruvate carboxykinase 1* (*pepck1*) (Miyamoto and Amrein, 2019). The results of our real-time quantitative reverse transcription PCR (qRT-PCR) analyses indicated that the transcription levels of *fbp* and *pepck1* were not significantly different between control flies under sated and starved conditions (***Figure 5A***). Next, we analyzed two lipogenic genes: *acetyl–CoA carboxylase* (*acc*) and *desaturase 1* (*desat1*) (***Figure 5A***) (Wang et al., 2022; Yee et al., 2013). No significant differences were identified between the control and $trp\gamma^{1}$ flies under both conditions. Finally, we investigated the expression of the lipolytic gene *brummer* (*bmm*) (***Figure 5A***) (Blumrich et al., 2021). Under starved conditions, the transcriptional level of *bmm* was highly increased in the control. In contrast, *bmm* was downregulated in $trp\gamma^{1}$ under sated and starved conditions. Therefore, the transcriptional regulation of w^{1118} and $trp\gamma^{1}$ during starvation was markedly and significantly different. The data indicates that the $trp\gamma$ mutant can sense the starvation state but responds abnormally by suppressing lipolysis instead of activating it. This dysregulated lipolytic response likely increases the mutant's vulnerability to starvation, as it cannot effectively mobilize lipid stores for energy during periods of nutrient deprivation. Brummer, a homolog of human adipocyte triglyceride lipase (ATGL), is associated with lipid storage in the form of LDs (Grönke et al., 2005; Men et al., 2016). These results suggest that the lipolytic process is not sufficient to deplete stored lipids in the $trp\gamma^{1}$ mutant, resulting in excessive lipid storage. Therefore,

the survival time of the *trpγ*^{1} mutant during starvation was significantly shorter than that of the control.

Transgenic flies expressing *bmm*::*GFP* (*bmm* promoter *GFP*) in their FB cells were used to examine *bmm* expression in LDs (Men et al., 2016). The fluorescent images obtained from the transgenic flies were then used to confirm our qRT-PCR results. Two images of control flies under sated and starved conditions were first analyzed both qualitatively and quantitatively (***Figure 5B and C***). Next, *trpγ*^{1} was analyzed under the two conditions (***Figure 5B and C***). A reduction in fluorescent intensity was clearly detectable in the *trpγ*^{1} mutant using the transgenic reporter line. These results further confirmed that *trpγ*^{1} has aberrant regulation in the lipolytic pathway.

To further substantiate the idea that the reduction in the expression level of *bmm* is the primary cause of the enlarged LDs in *trpγ* mutant flies, we measured LDs in the FB after expressing *UAS-bmm* using specific *GAL4* drivers: *trpγ*^{G4}*, Dh44-GLA4, r4-GAL4* (fat body specific)*, Myo1A-GAL4* (gut enterocyte specific), and *Dmef-GAL4* (muscle specific). Only *trpγ*^{G4}*, Dh44-GAL4* and *r4-GAL4* were able to restore the enlarged LDs defects in the FB, as well as TAG levels of whole body, after expressing *UAS-bmm* (***Figure 5D–J and Figure 5–figure supplement 1***). These findings suggest that the downregulation of *bmm* is one of the factors contributing to the elevated lipid defects in *trpγ*^{1}. Furthermore, the expression of *bmm* in the fat body, as well as *Dh44* neurons in the PI region, can promote lipolysis at the systemic level.

To conclusively explore whether metformin targets enzymes involved in lipid metabolism, specifically lipolytic or lipogenic genes, we administered 5 mM metformin

supplemented in normal food for one day and measured the expression levels of *bmm*, *acc*, and *desat1*. Oral supplementation of metformin resulted in an increase in the expression level of the lipolytic gene, *bmm* lipase of the control as well as *trpγ*^{1} (***Figure 5K***). Importantly, there was no observed effect of metformin on the expression levels of lipogenic genes. This data provides insights into the mode of action of metformin, suggesting a specific impact on lipolysis.

Recovery of the TRPγ mutant through oral lipase administration or lipid absorption

The intestine is a key organ for lipid absorption and metabolism (Han et al., 2020) and disturbances in intestinal lipid metabolism are associated with hyperlipidemia (Jia et al., 2021). To clarify if our observations were due to insufficient activity of lipase in the gut, lipase enzyme mixed with 1% agar food was supplied to both control and mutants flies. Given that the brief activity of lipase in the intestine, lipase-containing agar food was provided to the flies every 12 h. Surprisingly, supplementation with lipase, but not denatured lipase, under starvation conditions increased the survival of *trpγ* mutant flies to levels comparable to those of the control flies (***Figure 6A***; LT_{50} of lipase treated-control and *trpγ*^{1}: 50.35 ±0.93 h and 44.94 ±1.33 h, respectively). To support the hypothesis that the extended lifespan of mutant flies during starvation is associated with dietary lipase intake, we examined lipid accumulation (***Figure 6–figure supplement 1A–E***). Lipase treatment resulted in the breakdown of lipid deposits in the mutant R2 region of intestine. Importantly, only active lipase showed an enhanced survival time under starvation conditions in mutant flies, while denatured lipase did not exhibit this

effect. Therefore, our findings suggest that lipase may play a role in digesting accumulated lipid in the intestine, though the mechanisms of lipase absorption remain unclear.

Next, we sought to assess the involvement of each of the components of TAG in the recovery of starvation susceptibility. TAG is composed of glycerol and three fatty acids. Therefore, we first fed the flies with 1% glycerol only. Glycerol extended the survival of the control and *trpγ*^{1} flies by 3–4-fold (***Figure 6B***). However, the LT_{50} of the control and *trpγ*^{1} were still significantly different (***Figure 6C***; LT_{50} of control and *trpγ*^{1}: 244.5 ± 20.10 h and 117.75 ± 3.32 h, respectively). Next, the flies were fed with 0.2% and 0.5% hexanoic acid (HA) (***Figure 6C and Figure 6–figure supplement 1F***; 0.2% HA, LT_{50} of control and *trpγ*^{1}: 65.44 ± 1.94 h and 52.32 ±2.05 h, respectively; 0.5% HA, LT_{50} of control and *trpγ*^{1}: 56.27 ±1.30 h and 46.27 ±1.47 h, respectively). Additionally, we also tested the effects of 0.2% and 0.5% concentrations of a TAG mixture (combination of mono-, di-, and tri- acylglycerol) (***Figure 6D and Figure 6–figure supplement 1G***; 0.2% TAG, LT_{50} of control and *trpγ*^{1}: 52.93 ±5.12 h and 50.1 ±3.74 h, respectively; 0.5% TAG, LT_{50} of control and *trpγ*^{1}: 65.1 ±2.6 h and 57.75 ±3.32 h, respectively). The HA and mixed TAG treatments significantly extended the survival of the *trpγ*^{1} mutants, albeit not to levels similar to those of the control. This indicated that the TRPγ mutants could not fully absorb and burn the digested lipid. Furthermore, lipid-only dietary supplementation markedly limited the LT_{50} of the control. Importantly, supplementation with lipolytic drugs, lipase, TAG, and free fatty acids effectively rescued the survival of *trpγ* mutants under starvation conditions. This observation was consistent with our finding that *trpγ* mutants

are unable to degrade lipid stores under starvation conditions. The dietary rescue of *trpγ* mutants suggests that although the *trpγ* mutation increases the levels of stored lipids, the flies were not able to utilize them when starved. We next sought to determine whether *trpγ* mutation reduces lipase production in the abdomen by comparing lipid accumulation in the intestine. The Drosophila midgut is divided into R1–R5 regions, each with distinct functions in nutrient processing and absorption. Notably, the R2 region serves as a critical interface between the fly's diet and metabolic processes (Capo et al., 2019). To assess lipid distribution, we conducted Nile red staining in control and mutant animals (***Figure 6E–H***). Mutant flies displayed elevated lipid deposits on the intestinal wall of the R2 region ***(Figure 6F***), a phenotype restored to normal levels by expressing *trpγ* in its own cells or *Dh44* neurons (***Figure 6G–I***). Consequently, we quantified lipid droplets specifically within the intestinal wall of the R2 region in $trp\gamma^{1}$ flies, with no such accumulation observed in control or rescued flies (***Figure 6I***). These findings indicate that TRPγ plays a crucial role in the brain-gut axis, specifically in controlling lipid metabolism in the intestine, as evidenced by the lipid accumulation observed in the gut region of $trp\gamma^{1}$. Taken together, these observations indicate that TRPγ plays an important role in maintaining systemic lipid levels through proper expression of triglyceride lipase.

Assessment of the role of DH44 and its receptors (DH44R1 and DH44R2) in relation to the utilization of fat

In Drosophila, two receptors have been identified for DH44 (Hector et al., 2009). In order to investigate the potential roles of DH44 in fat utilization and identify the receptor responsible for nutrient regulation, we examined lipid and protein levels in *Dh44*^{Mi}, *Dh44R1*^{Mi}, and *Dh44R2*^{Mi}. *Dh44*^{Mi} and *Dh44R1*^{Mi} showed normal total TAG levels, while *Dh44R2*^{Mi} exhibited higher lipid levels like *trp*γ^{1} (***Figure 7A***). Additionally, Nile red staining of LDs in the FBs revealed that *Dh44*^{Mi} and *Dh44R2*^{Mi} mutants possessed larger LDs (***Figure 7B–F***), although protein levels remained unaffected across all three mutants (***Figure 7G***). Further investigations quantified the expression of the *bmm* in the FBs of *Dh44*^{Mi}, *Dh44R1*^{Mi}, and *Dh44R2*^{Mi} under both sated and starved conditions. In sated conditions, *bmm* expression was found to be downregulated in *Dh44R2*^{Mi} compared to the control (***Figure 7H***). Interestingly, under starved conditions, while *bmm* levels significantly increased in the control, indicating a normal response to starvation, such an increase was not observed in *Dh44*^{Mi} and *Dh44R2*^{Mi}. Instead, in these mutants, *bmm* levels significantly decreased compared to their levels under sated conditions (***Figure 7H***). In addition, *bmm* levels in *Dh44R1*^{Mi} under starved condition did not increase as significantly as in the control. This suggests a unique role of DH44 and its receptors in regulating lipid metabolism and response to nutritional status in *Drosophila*.

To further verify whether *Dh44*, *Dh44R1*, and *Dh44R2* mutants can be recovered by oral lipase administration or lipid absorption, we measured the starvation survival time with 1% agar and 1% agar with 0.1% lipase, 1 % glycerol, 0.2 % HA, and 0.2 % mix TAG (***Figure 7–figure supplement 1A–D***). Under starvation condition, *Dh44*^{Mi} and *Dh44R2*^{Mi} showed significantly reduced survival time compared to control, whereas *Dh44R1*^{Mi} flies were normal (LT_{50} of control, *Dh44*^{Mi}, *Dh44R1*^{Mi}, and *Dh44R2*^{Mi}: 54.32 ±

2.29 h, 36.95 ± 1.76 h, 46.83 ± 1.27 h, and 36.33 ±1.03 h respectively). Interestingly, the reduced survival time observed in *Dh44*^{Mi} and *Dh44R2*^{Mi} mutants were improved with the supplementation of lipase (LT_{50} of *Dh44*^{Mi} and *Dh44R2*^{Mi}: 54.72 ± 0.55 h and 48.63 ± 1.18 h), glycerol (LT_{50} of *Dh44*^{Mi} and *Dh44R2*^{Mi}: 239 ± 1.91 h and 238.5 ± 5.12 h) , hexanoic acid (LT_{50} of *Dh44*^{Mi} and *Dh44R2*^{Mi}: 62.50 ± 1.50 h and 58.77 ± 0.81 h), and mixed TAG (LT_{50} of *Dh44*^{Mi} and *Dh44R2*^{Mi}: 54.70 ± 3.53 h and 59.50 ± 2.06 h) (***Figure 7–figure supplement 1A–D***).

To explore the connection between TRPγ and DH44 signaling, we expressed *UAS-trpγ* under the control of *Dh44R1-GAL4* and *Dh44R2-GAL4*. Only *Dh44R2-GAL4* restored the lipid defect in *trpγ*^{1}, unlike *Dh44R1-GAL4* (***Figure 7I***). Furthermore, *Dh44R2-GAL4*, but not *Dh44R1-GAL4*, rescued the excessive lipid accumulation in the FB of *trpγ*^{1} mutants (***Figure 7J–N***). Given that *Dh44R2* is predominantly expressed in the intestine, we performed immunostaining to examine whether *Dh44R2* co-localizes with *trpγ* in gut cells. Our results confirmed that *Dh44R2* and *trpγ* are co-expressed in intestinal cells (***Figure 7O and P***). Additionally, we analyzed *Dh44R2* expression in the brain and found that two *Dh44R2*-expressing cells are co-localized with *Dh44*-expressing cells in the PI region (***Figure 7Q***). To further delineate whether *Dh44R2*-mediated fat utilization is specific to the brain, gut, or fat body, we knocked down *Dh44R2*^{RNAi} using *Dh44-GAL4*, *Myo1A-GAL4*, and *cg-GAL4*, respectively (***Figure 7–figure supplement 1E***). Notably, knockdown of *Dh44R2* with *Myo1A-GAL4* resulted in elevated TAG levels, indicating that DH44R2 activity in lipid metabolism is specific to the gut.

DISCUSSION

Here, we found that the function of TRPγ, one of the TRPC channels of *D. melanogaster*, in DH44 neuroendocrine cells plays an essential role in lipid regulation, which is linked to alterations in membrane lipids (Cobb et al., 2021; Overgaard et al., 2005). The *trpγ*^{1} mutant exhibited clear signs of metabolic syndrome, as demonstrated by reduced carbohydrate level coupled with much higher protein and lipid levels in the body (***Figure 8***). More importantly, we found that the expression of *trpγ* in DH44 neurons was necessary and sufficient to regulate the carbohydrate and lipid. However, we failed to identify the specific cells required for regulating protein homeostasis because the increased protein levels in the *trpγ* mutants were not recovered by pilot screening (data not shown) except in the *trpγ-GAL4*. In conclusion, our findings suggested that the DH44 system has important roles in regulating the metabolic homeostasis of carbohydrates and lipids (***Figure 8***).

The metabolic dysregulation of carbohydrates and lipids observed in the *trpγ* mutants was phenocopied by the cellular inactivation of DH44 cells. Compared to the controls, the *Dh44-GAL4*/*UAS-Kir2.1* flies exhibited lower carbohydrate levels and increased lipid levels. We previously proposed that TRPγ holds DH44 neurons in a state of afterdepolarization, thus reducing firing rates by inactivating voltage-gated Na^{+} channels (Dhakal et al., 2022). At the physiological level, this induces the consistent release of DH44 and depletion of DH44 stores, resulting in nutrient utilization and storage malfunctions. Likewise, our findings revealed that *Dh44* mutant and its receptor mutant, *Dh44R2*, displayed defects analogous to those observed in the *trpγ* mutant. The

trpγ mutant phenotype in lipid regulation can be restored by the expression of *trpγ* in the *Dh44-GAL4* as well as *Dh44R2-GAL4*. This indicates that TRPγ function in the brain and gut independently for lipid homeostasis. The mode of action for TRPγ in the gut should be further investigated. Finally, it would also be interesting to investigate the potential roles of TRPC members in humans, especially the involvement of TRPC4 and TRPC5 in metabolic syndrome.

Multiple lines of evidence have suggested that DH44 neurons communicate with the intestine. First, DH44 at the PI in the brain is an incretin-like hormone that acts as a hemolymph nutrient sensor. The secretion of DH44 is highly dependent on the calorie value of a given diet, as DH44 secretion is only mediated by nutritional sugars but not non-nutritional sugars (Dhakal et al., 2022; Dus et al., 2015; Oh et al., 2021). Second, the expression of TRPγ in the PI is sufficient to recover any metabolic defects such as reduced carbohydrate and increased lipid levels, as well as related phenomena such as starvation resistance. DH44 and kinin neuropeptides influence desiccation and starvation tolerance in *D. melanogaster* (Cannell et al., 2016). There is an inconsistency of total TAG levels and the LD size observed in the *Dh44* mutant. This inconsistency raises a possibility that the signaling pathway from DH44 release to its receptor DH44R2 only accounts for part of the lipid metabolic process under starvation. While *Dh44* mutant flies displayed normal internal TAG levels, *Dh44R2* mutant flies exhibited elevated TAG levels. This suggested that the lipolysis phenotype could be facilitated by a neuropeptide other than DH44. Alternatively, a DH44 neuropeptide-independent pathway could mediate the lipolysis. Although $Dh44^{Mi}$ exhibited normal TAG levels, the presence of larger LDs indicated that DH44 plays a regulatory role in lipid metabolism.

LDs consist of a hydrophobic core of neutral storage fats, such as triglycerides or cholesterol esters, encased by a protein-coated phospholipid monolayer. From our findings, it is suggested that DH44 and its receptor DH44R2, but not DH44R1, are involved in the control of lipid storage, indicating a specific pathway through which DH44 influences lipid metabolism distinct from its role in carbohydrate metabolism and overall energy homeostasis. TRPγ in DH44 neurons may influence the release of metabolic signals or hormones that act on postsynaptic DH44R2 cells. These postsynaptic cells could, in turn, modulate lipid storage and metabolism in a non-cell autonomous manner. However, the mechanism by which TRPγ functions in DH44R2 cells remains unclear. One possible explanation is that TRPγ in the gut may be activated by stretch or osmolarity (Akitake et al., 2015). Third, *trpγ* gene knockdown through RNAi in the DH44 neurons is enough to phenocopy all of the metabolic defects observed in the *trpγ* mutants. Fourth, *trpγ* mutants exhibit low expression of *brummer* lipase, which results in accumulation of LDs in the body, which is a reciprocal process regulated by DH44 neurons. Brummer lipase is essential for regulating lipid levels in the insect fat body by mediating lipid mobilization and energy homeostasis. In *Nilaparvata lugens*, it facilitates triglyceride breakdown (Lu et al., 2018), while studies in *Drosophila* show that reduced Brummer lipase expression decreases fatty acids and increases diacylglycerol levels, highlighting its role in lipid metabolism (Nazario-Yepiz et al., 2021). Here, we additionally demonstrate that *bmm* expression in DH44 neurons within the PI region can systemically regulate TAG levels. Cell signaling or energy status in DH44 neurons may contribute to hormonal release that targets organs such as the fat body. Fifth, the activation of AMPK in the DH44 neurons can recover the defects of lipid level

of *trpγ*^{1}. Sixth, the reduced starvation resistance can be significantly recovered through dietary lipase supplementation. These findings support the assertion that the sugar-sensing DH44 neurons send downward signals to the intestine by absorbing the carbohydrates and lipids derived from dietary intake. However, DH44 neurons do not regulate protein levels in the body because the increased protein levels of *trpγ* mutants were not recovered by the expression of *trpγ* in the DH44 neurons. These findings confirm that *trpγ* regulates *bmm* expression in the adult bowel, enabling dietary lipid digestion and maintaining systemic lipid homeostasis.

Treatment with metformin, a lipolytic agent, at two different concentrations (1 mM and 5 mM) decreased the total TAG levels and reduced the size of the LDs in *D. melanogaster*. Similarly, metformin increased the starvation resistance of the *trpγ*^{1} mutants but not the controls. These findings were consistent with the widely acknowledged anti-obesity properties of metformin (Sang et al., 2021). Furthermore, our results were in agreement with the evidence that metformin helps to reduce lipid accumulation caused by diets rich in saturated fatty acids (Kim et al., 2020). Although the exact target of metformin is not known, its lipolytic effect is significant and widely documented. Oral administration of 5 mM of metformin reduced normal TAG levels of wild-type flies, whereas the 1 mM dose had no significant effect. Therefore, low metformin doses were effective at decreasing stored lipid levels in flies. The accumulation of intracellular LDs is regulated by autophagy. Metformin improves autophagic flux through AMPKα-mediated mechanisms (Kim et al., 2020). In the *Drosophila* context, we propose a mechanism involving AMPK activation within DH44

neurons as a rescue mechanism for starvation resistance in *trpγ*^{1}, highlighting its crucial role in this process. AMPK activation is known to enhance an organism's ability to endure environmental stresses by facilitating autophagy-mediated cellular cleanup, promoting mitochondrial biogenesis for increased energy production, and optimizing metabolic pathways for enhanced energy efficiency (Kim et al., 2020). While the precise nature of the connection between TRPγ, DH44 neuronal activity, and AMPK activation remains unspecified, it is conceivable that TRPγ influences AMPK activation or regulation within DH44 neurons, contributing to stress responses, ATP supply, and metabolic adaptations. Metformin can influence lipid metabolism through various mechanisms, one of which is the promotion of lipolysis (Szkudelski et al., 2022). This effect results in a gradual reduction of stored lipid levels over time. Orally administering metformin to flies led to a significant reduction in lipid levels, accompanied by an increase in survival. Subsequent qPCR analysis post-metformin feeding revealed a significant upregulation in the expression level of the lipolytic gene (*bmm*). These results strongly support our hypothesis that metformin induces lipolysis when orally administered.

The exact mechanism through which orally administered lipase leads to gastric lipolysis remains unclear. However, our experimental data indicated that 0.1% lipase increased the survival time of *trpγ*^{1} under starvation. Lipase exhibits a high degree of chemical selectivity and has the ability to catalyze triglyceride into glycerol ester, monoglycerides, glycerol, and fatty acids (Liu et al., 2020). Free fatty acids, HA, and glycerol at concentrations of 0.2%–0.5% can be utilized as energy sources and increase

survival time under starvation conditions, suggesting that *trpγ*^{1} participates in the utilization of HA and glycerol under starvation conditions.

The therapeutic properties of metformin as a lipolytic and anti-diabetic drug have been widely documented in humans. However, additional studies are needed to identify the exact target of metformin. In this context, our findings demonstrate that *D. melanogaster* can be an excellent model to study the mode of action and biosafety of metformin.

MATERIALS AND METHODS

Key resources table

REAGENT or RESOURCE	SOURCE	IDENTIFIER
Mouse anti-GFP	Molecular probe	Cat # A11120
Rabbit anti-DsRed	Takara	Cat # 632496
Goat anti-mouse Alexa Fluor 488	Thermo Fisher/Invitrogen	Cat # A11029
Goat anti-mouse Alexa Fluor 568	Thermo fisher/Invitrogen	Cat # A11004
Rabbit anti-Dh44	Dr.J.A. Veenstra	NA
Goat anti-rabbit Alexa Fluor 488	Thermo fisher/Invitrogen	Cat # A11034
Goat anti-rabbit Alexa Fluor 568	Thermo fisher/Invitrogen	Cat # A11036
Chemicals, peptides, and recombinant proteins		
Trehalase from porcine kidney	Sigma-Aldrich Co.	Cat # 9025-52-9
Amyloglucosidase from Aspergillus	Sigma-Aldrich Co.	Cat # 9032-08-0
Glucose (HK) Assay Kit	Sigma-Aldrich Co.	Cat # GAHK-20
Glucose (HK) Assay reagent	Sigma-Aldrich Co.	Cat # G3293
The Pierce™ BCA protein assay kit	Thermo Fischer Scientific	Cat # 23225
Triglyceride mix	Sigma-Aldrich Co.	Cat #17810-1AMP-S
LiquiColor triglyceride test kit	Stanbio Laboratory	Cat # 2100-225
Lipase from *Candida rugosa*	Sigma-Aldrich Co.	Cat # L1754
Metformin	Sigma-Aldrich Co.	Cat # D150959
Hexanoic acid	Sigma-Aldrich Co.	Cat # W255912
Sucrose	Sigma-Aldrich Co.	Cat # 57-50-1
LiquiColor Triglyceride Test kit	Stanbio Laboratory	Cat # 2100-225
Glycerol	Sigma-Aldrich Co.	Cat # G5516
Nile red	Sigma-Aldrich Co.	Cat # N3013
Experimental models: Organisms/strains		
Genotype	Source	Identifier
trpγ^{1}	Dr. C. Montell	BDSC:64311
trpγ^{G4}	Dr. C. Montell	BDSC:64313
trpγ^{1}*,UAS-trpγ/CyO*	Dr. C. Montell	(Akitake et al., 2015)
trpγ^{1};g(*trpγ*)	Dr. C. Montell	(Akitake et al., 2015)
trpA1^{1}	Dr. C. Montell	BDSC:26504
amo^{1}	Dr. C. Montell	(Watnick et al., 2003)
trpml^{2}	Dr. C. Montell	BDSC:42230
trp^{343}	Dr. C. Montell	BDSC:25082
pyx^{3}	Dr. Y. Lee	(Lee et al., 2005)
wtrw^{ex}	Dr. C. Montell	BDSC:59038
trpl^{29134}	Bloomington Drosophila Stock center	BDSC:29134
iav^{3621}	Bloomington Drosophila Stock center	BDSC: 24768
pain^{2}	Dr. S. Benzer	(Tracey Jr et al., 2003)

nan^{36a}	Dr. C. Kim	(Kim et al., 2003)
diLP2-GAL4	KDRC	KDRC: 200
Dh44-GAL4	Dr. Y. Kim	KDRC: 2543
UAS-mCD8::*GFP*	Bloomington Drosophila Stock Center	BDSC: 5130
UAS-Kir2.1	Bloomington Drosophila Stock Center	BDSC: 6596
UAS-trpγ^{RNAi}	Bloomington Drosophila Stock Center	Transformant ID107656
r4-GAL4	Korea Drosophila Resource Center	GIST: 2166
cg-GAL4	Dr. S. Hyun	BDSC: 7011
Myo1A-GAL4	Dr. S. Hyun	BDSC: 67057
Dmef-GAL4	Dr. S. Hyun	BDSC: 27390
UAS-AMPK^{TD}	Korea Drosophila Resource Center	KDRC:10099
UAS-bmm	Bloomington Drosophila Stock Center	BDSC: 76600
Dh44^{MI}	Dr. Y. Kim	BDSC: 24345
Dh44R1^{MI}	Dr. Y. kim	BDSC: 23517
Dh44R2^{MI}	Dr. Y. Kim	BDSC: 29129
Dh44R1-GAL4	Dr. Y. Kim	KDRC: 2734
Dh44R2-GAL4	Dr. Y. Kim	BDSC: 66865
Dh44R2^{RNAi}	Korea Drosophila resource center	KDRC: 5121
yw;+;bmm::*GFP*	Dr. Kaeko Kamei	(Men et al., 2016)
Dh44-LexA	Korea Drosophila Resource Center	KDRC 2776
Dh44R2-LexA	Korea Drosophila Resource Center	KDRC 6616
LexAop-mCherry	Korea Drosophila Resource Center	KDRC 1247
Software and algorithms		
Origin Pro Version	OriginLab corporation	RRID: SCR_002815 https:/www.originlab.com
Graphpad Prism	GraphPad	RRID: SCR_002798 https:/www.graphpd.com
Fiji(ImageJ-win64)	https://fiji.sc	

Chemical sources

Trehalase from porcine kidney (cat. # 9025-52-9), amyloglucosidase (cat. # 9032-08-0), the glucose (HK) assay kit (cat. # GAHK-20-1KT), and triglyceride mix (cat. # 17810-1AMP-S), lipase from *Candida rugosa* (cat. # OT705690000), metformin (cat. # D150959), Nile Red (cat. # N3013), glycerol (cat. # G5516) were purchased from Sigma-Aldrich Co. Hexanoic acid (cat. # W255912) were purchased from Wako Pure

Chemical Industry Ltd. The Pierce™ BCA protein assay kit (cat. # 23225) and the LiquiColor triglyceride test kit (cat. # 2100-225) were purchased from Thermo Fisher Scientific and Stanbio Laboratory, respectively.

TAG level measurement

TAG levels were quantified as described previously with some modifications using a LiquiColor Triglyceride Test kit (cat. # 2100-225, Stanbio Laboratory, Germany) (Sang et al., 2021). Ten 5–10 day-old male flies were weighed and crushed in 1 mL of PBST (1X PBS and 0.2 percent Triton X-100). The homogenate was incubated at 70 °C for 5 minutes and centrifuged for 3 minutes at 9,500 g. Next, 100 µL of supernatant was transferred into a 1.5 mL Eppendorf tube and mixed with 1 mL of Stanbio LiquiColor Triglyceride Test kit reagent or 1 mL of deionized water to provide a baseline. The reaction mixture was kept at 37 °C for 15 minutes. Finally, the absorbance of the sample solution was measured at 500 nm using a spectrophotometer and the TAG level was calculated based on a standard calibration curve.

Protein level measurement

Protein assays were performed as previously described using the Pierce™ BCA Protein Assay Kit with some modifications. Briefly, ten 5–10 day-old male flies were weighed and crushed in 1 mL of PBST (1X PBS and 0.2 percent Triton X-10) and incubated at 70 °C for 5 minutes. The homogenate was then centrifuged for 3 minutes at 9,500 g, after which 300 µL of supernatant was mixed with 600 µL of Pierce™ BCA Protein

Assay Kit (UF289330). After a 30-minute incubation period at 37 °C, the absorbance of the samples was measured at 530 nm using a spectrophotometer and compared to a standard calibration curve for quantification.

Trehalose and glucose measurements in whole adult flies or hemolymph

Whole-body glucose and trehalose levels were measured in adult flies as previously described (Meunier et al., 2007). Briefly, ten 5–10 day old males were collected, weighed, and crushed in 250 µL of 0.25 M Na_2CO_3 buffer. The homogenates were then incubated in a water bath (95°C) for 5 min to inactivate all enzymes. Next, 600 µL of 0.25 M sodium acetate and 150 µL of 1 M acetic acid (pH 5.2) were added to the samples, after which the mixtures were centrifuged at 12,500 *g* for 10 min at 24 °C. Afterward, 200 µL of supernatant was transferred a new microfuge tube and 2 µL porcine kidney trehalase (Sigma: T8778 UN) was added to the sample mixture and incubated overnight at 37 °C to convert trehalose into glucose. Next, 1 mL of glucose hexokinase solution (Sigma: GAHK-20) was added to 100 µL of the sample and incubated for 20 min at 37 °C. Optical density (OD) values were measured at 340 nm. Finally, total glucose and trehalose levels were calculated using a standard glucose curve generated through similar reactions with standard trehalose and glucose.

Glucose and trehalose level measurement in hemolymph were extracted from the male flies. Flies were punctured in the thorax with the help of fine injection needle and kept in 0.5 mL tubes having a punctured base with 21-gauge needle. The punctured flies were adjusted by keeping the shoulder down to prevent leakage from

the genital tract. The tubes were set into the 1.5 mL microfuge tube and centrifuged at 4°C for 5 minutes at 2800 g force. 0.5 µL of hemolymph was added to 14.5 µL PBS. 2 µL of porcine kidney trehalase (Sigma: T8778 UN) was added to the sample mixture and incubated overnight at 37°C to convert trehalose into glucose. 1 mL of glucose hexokinase solution (Sigma: GAHK-20) was added to the 100 µL of the sample and incubated at 37°C for 20 minutes. Optical density (OD) values were measured at 340 nm. Total glucose and trehalose levels were calculated using a standard glucose curve generated through similar reactions with standard trehalose and glucose.

Glycogen measurements

Tissue glycogen levels from whole-body extracts of adult flies were quantified as previously described (Dus et al., 2011). Briefly, 5 males were homogenized in 100 µL of ice-chilled 1X PBS after measuring the weight. The homogenates were kept at 70 °C for 5 min to inactivate all metabolic enzymes. The homogenates were then centrifuged at 12,500 *g* for 3 min at 4 °C, after which 20 µL of the supernatant was transferred to 1.5 mL microfuge tubes and diluted with 1X PBS to a 1:3 ratio. An amyloglucosidase dilution was prepared by mixing 1.5 µL of amyloglucosidase (Sigma A1602) suspension in 998.5 µL 1X PBS. Finally, a 20 µL aliquot of the diluted sample was added to 20 µL of the diluted amyloglucosidase solution, as well as to the glycogen standard. Both the glycogen standard and test samples were then incubated at 37 °C for 1 h. A commercial glucose (HK) assay reagent (Sigma: G3293 VER) was used to measure total glucose at 340 nm. The glycogen level was quantified by comparing it with standard curve plotted from standard glycogen samples.

Survival assay

Survival experiments were conducted as previously described (Lee et al., 2018). Normal cornmeal diets were used to conduct the normal survival assays. To measure survival under starvation conditions, twenty 3–4-day-old male flies were fed with 1% agar food supplemented with or without various concentrations of lipase (0.1%; active or denatured), glycerol (1%), hexanoic acid (0.2%, 0.5%), glycerol (1%), TAG mix (0.2%, 0.5%), or metformin (1 mM, 5 mM). Every 12 hours, the flies were monitored/counted and then transferred to fresh vials with the same food supply. The experiments were conducted until the food vials had been cleared.

Immunohistochemistry

We performed immunohistochemistry as previously described (Dhakal et al., 2022). Briefly, to fix and block the specimens, we placed freshly dissected tissues (brain and intestine) into a well of 24-well tissue culture plate (Costar Corp.) placed on ice, which contained 940 µL of fixing buffer (1 mM EGTA, 0.1M Pipes pH 6.9, 2 mM $MgSO_4$, 1% TritonX-100, 150 mM NaCl). 60 µL formaldehyde (37%) was added to the wells and mixed instantly before the tissues were added. As many as tissues that were dissected within 15 minutes were fixed and then the samples were incubated for 30 min more. Samples were washed with wash buffer (1X PBS, 0.1% saponin) three times (15 min. for each washing), and blocked with 1 mL blocking buffer (1X PBS, 0.1% saponin, and 5 mg/mL BSA) at 4 °C for 4-8 hours.

To perform immunostaining, primary antibodies were inserted into the sample at 4°C for 18 hours (Jais and Brüning, 2022). Samples were washed with wash buffer three times (15 min each) and added secondary antibodies {(1:200) goat anti-mouse Alexa Fluor 488 (cat. # A11029), goat anti-mouse Alexa Fluor 568 (cat. # A11004), goat anti-rabbit Alexa Fluor 488 (cat. # A11034), and goat anti-rabbit Alexa 568 (cat. # A11036) at 4 °C for 4 hours. Finally, samples were washed three times and stored into 1.25X PDA (187.5 mM NaCl, 37.5% glycerol, 62.5 mM Tris pH 8.8), and kept at 4°C for more than 1 hr. Samples were mounted and examined using a Leica Stellaris 5 Confocal Microscope.

Nile red staining

Nile Red is a dark purplish-red powder (Sigma N-3013), the stock solution must be prepared in acetone (1000 µg/mL) and kept in a tightly sealed, lightproof container at 4 °C. Briefly, 5–10 day-old male flies were fixed in a sagittal position on a glass slide and submerged in a 1 X PBS solution. FBs were gently dissected from a dorsal abdominal region along with thorax or the gut under a stereomicroscope. The dissected tissues were fixed with 4% formaldehyde solution for 15 minutes at room temperature. The fixed tissues were gently washed three times with 1X PBS (5 min for each wash). Nile Red (1:1000 dilution) were added to the tissue samples for 5 minutes. Finally, the stained tissues were washed with 1 mL 1X PBS and mounted in 50% glycerol on a glass slide. LD deposition exhibits greater density in the upper abdominal region compared to the lower abdominal area. This comparison was meticulously conducted within the identical segments 2-3 of the abdomen to ensure accuracy.

For intestinal lipid staining, 5-10 days old male flies were fixed on a glass slide and submerged in 1X PBS solution. Full intestine was dissected very carefully. The dissected intestine was fixed with 4% formaldehyde solution for 15 minutes at room temperature. The fixed intestine was washed 3 times with 1X PBS. Nile red was added to the sample for 5 minutes. The stained samples were washed with 1mL 1X PBS and mounted in 50% glycerol on a glass slide. The stained tissues were examined using a Leica Stellaris 5 Confocal Microscope.

qRT-PCR

qRT-PCR assays were performed as described previously (Yoshinari et al., 2021). Briefly, ten 6–10 day-old male flies (control and mutant) were selected for whole body and 15 flies were selected for fat body samples in Supplement Figure 6K. The experiments were conducted under sated (0 h starvation) and starved (24 h starvation) conditions. Total RNA was extracted using the TRizol reagent (Invitrogen) followed by DNase (Promega) treatment. cDNA was synthesized using the AMV reverse transcriptase system (Promega). RT-qPCR experiments were carried out using a Bio-rad CFX system. The Takara TB Green Premix was used to assess the mRNA expression level of each gene according to the manufacturer's instructions. Relative gene expression was calculated using the $2^{-\Delta\Delta Ct}$ method. Three biological samples were used and transcript levels were normalized to the *D. melanogaster* housekeeping gene *tubulin*. The experiments were conducted using the following primer pairs: *acc*, 5'-ACG AGG GCG AGC AGC GTT AC-3′ (forward) and 5′-TAG GGC GAC TTG GTG GGC AT-

3′ (reverse); *bmm*, 5′-ATG ACT TCG GAC TTC TTC AGG G-3′ (forward) and 5′-CCA ATT CAG ATG GAA GAG CTG-3′ (reverse); *fbp*, 5′-CTC CAA CGA GCT GTT CAT CA-3′ (forward) and 5′-TGA ACC GAT CGA CAC CAG GC-3′ (reverse); *pepck1*, 5′-AGG TGC ACA TCT GCG ATG GC-3′ (forward) and 5′-CCA CCA CGT AAG CAG AGT CC-3′ (reverse); *desat1*, 5'-AAG CCG GTG CCC AGT CCA TC-3' (forward) and 5'-ATG GTC GCG AGC CCA ATG GT-3' (reverse); and *tubulin*, 5′-TCC TTG TCG CGT GTG AAA CA-3′ (forward) and 5′-CCG AAC GAG TGG AAG ATG AG-3' (reverse).

Statistics and Reproducibility

D. melanogaster was selected as a model organism in this study. For the experiments, male flies were mostly used unless we did not mention the sex. All of the experiments were conducted under laboratory conditions. The appropriate number of replicates was established based on previous research. A large enough sample size was used in all of our assays to ensure that our results were representative and repeatable. No data points were left out of the analysis. For each genotype, the data points indicate the values of individual replicates. The error bars in all of the figures represent the standard error of the mean (SEM). The analysis of the RT-qPCR data was conducted using the C_T values. Comparisons between multiple experimental groups were conducted via single-factor ANOVA and Scheffe's *post hoc* test. Pair-wise comparisons were conducted via Student's t-test. Survival curves were estimated for each group, using a Kaplan-Meier method and compared statistically using the log-rank tests. The asterisks in the figures indicate statistical significance (*P<0.05, **P<0.01). All statistical analyses

were conducted using the Origin Pro 8 software for Windows (ver. 8.0932; Origin Lab Corporation, USA).

Competing interest statement

The authors have no competing interests.

Acknowledgments

This work was supported by grants to Youngseok Lee from the National Research Foundation of Korea (NRF) funded by the Korea government (MIST) (NRF-2021R1A2C1007628) and the Biomaterials Specialized Graduate Program through the Korea Environmental Industry & Technology Institute (KEITI) funded by the Ministry of Environment (MOE). D.K.N. and S.D. were supported by the Global Scholarship Program for Foreign Graduate Students at Kookmin University in Korea.

Author contributions

D.K.N. and S.D. performed the experiment, analyzed the data, generated the figures, and wrote the original draft. Y.L. supervised, reviewed and edited the draft, wrote the original manuscript, and obtained the funding.

Additional Information

Authors ORCIDS

Dharmendra Kumar Nath https://orcid.org/0000-0001-6105-6970

Dhakal Subash https://orcid.org/0000-0002-5380-1130

Youngseok Lee http://orcid.org/0000-0003-0459-1138

Additional files

Data availability

Source data for all figures contained in the manuscript and SI have been deposited in 'figshare' (https://doi.org/10.6084/m9.figshare.28029974).

Supplementary Files

Figure 2–figure supplement 1. Expression of trpγ, Dh44 and dilp2 in the brain of *Drosophila*.

Figure 3–figure supplement 1. Measurement of TAG levels after overexpressing *UAS-trpγ* and knock-down of $trp\gamma^{RNAi}$ in *Dh44* neurons.

Figure 5–figure supplement 1. Measurement of TAG levels after expressing *UAS-bmm* in $trp\gamma^{G4}$*, Dh44-GAl4, r4-GAL4 and Myo1A-GAL4*.

Figure 6–figure supplement 1. Measurement of lipase effect in LDs and starvation survival assay after feeding hexanoic acid or mixed TAG**.**

Figure 7–figure supplement 1. Measurement of starvation survival time with feeding lipase, glycerol, hexanoic acid and triglyceride mix in 1% agar food.

References

Akitake, B., Ren, Q., Boiko, N., Ni, J., Sokabe, T., Stockand, J.D., Eaton, B.A., and Montell, C. 2015. Coordination and fine motor control depend on *Drosophila* TRPγ. *Nature communications* **6**: 1-13. DOI: https://doi.org/10.1038/ncomms8288

Blumrich, A., Vogler, G., Dresen, S., Diop, S.B., Jaeger, C., Leberer, S., Grune, J., Wirth, E.K., Hoeft, B., and Renko, K. 2021. Fat-body brummer lipase determines survival and cardiac function during starvation in *Drosophila melanogaster*. *IScience* **24**: 102288. DOI: 10.1016/j.isci.2021.102288

Cannell, E., Dornan, A.J., Halberg, K.A., Terhzaz, S., Dow, J.A., and Davies, S.-A. 2016. The corticotropin-releasing factor-like diuretic hormone 44 (DH44) and kinin neuropeptides modulate desiccation and starvation tolerance in *Drosophila melanogaster*. *Peptides* **80**: 96-107. DOI: 10.1016/j.peptides.2016.02.004

Capo, F., Wilson, A., and Di Cara, F. 2019. The intestine of *Drosophila melanogaster*: An emerging versatile model system to study intestinal epithelial homeostasis and host-microbial interactions in humans. *Microorganisms* **7**: 336. DOI: 10.3390/microorganisms7090336

Clapham, D.E. 2003. TRP channels as cellular sensors. *Nature* **426**: 517-524. DOI: 10.1038/nature02196

Cobb, T., Damschroder, D., and Wessells, R. 2021. Sestrin regulates acute chill coma recovery in *Drosophila melanogaster*. *Insect biochemistry and molecular biology* **133**: 103548. DOI: https://doi.org/10.1016/j.ibmb.2021.103548

Dhakal, S. and Lee, Y. 2019. Transient receptor potential channels and metabolism. *Molecules and cells* **42**: 569-578. DOI: 10.14348/molcells.2019.0007

Dhakal, S., Ren, Q., Liu, J., Akitake, B., Tekin, I., Montell, C., and Lee, Y. 2022. *Drosophila* TRPγ is required in neuroendocrine cells for post-ingestive food selection. *Elife* **11**: e56726-e56726. DOI: https://doi.org/10.7554/eLife.56726

Dus, M., Lai, J.S.-Y., Gunapala, K.M., Min, S., Tayler, T.D., Hergarden, A.C., Geraud, E., Joseph, C.M., and Suh, G.S. 2015. Nutrient sensor in the brain directs the action of the brain-gut axis in *Drosophila*. Neuron **87**: 139-151. DOI: 10.1016/j.neuron.2015.05.032

Dus, M., Min, S., Keene, A.C., Lee, G.Y., and Suh, G.S. 2011. Taste-independent detection of the caloric content of sugar in *Drosophila*. *Proceedings of the National Academy of Sciences*. **108**: 11644-11649. DOI: https://doi.org/10.1073/pnas.101709610

Efeyan, A., Comb, W.C., and Sabatini, D.M. 2015. Nutrient-sensing mechanisms and pathways. *Nature* **517**: 302-310. DOI: https://doi.org/10.1038/nature14190

Fowler, M.A. and Montell, C. 2013. *Drosophila* TRP channels and animal behavior. *Life sciences* **92**: 394-403. DOI: 10.1016/j.lfs.2012.07.029

Grönke, S., Mildner, A., Fellert, S., Tennagels, N., Petry, S., Müller, G., Jäckle, H., and Kühnlein, R.P. 2005. Brummer lipase is an evolutionary conserved fat storage regulator in *Drosophila*. *Cell metabolism* **1**: 323-330. DOI: 10.1016/j.cmet.2005.04.003

Han, J., Guo, X., Meng, X.-J., Zhang, J., Yamaguchi, R., Motoo, Y., and Yamada, S. 2020. Acupuncture improved lipid metabolism by regulating intestinal absorption in mice. *World Journal of Gastroenterology* **26**: 5118. DOI: 10.3748/wjg.v26.i34.5118

Hardie, D.G., Scott, J.W., Pan, D.A., and Hudson, E.R. 2003. Management of cellular energy by the AMP-activated protein kinase system. *FEBS letters* **546**: 113-120. DOI: 10.1016/s0014-5793(03)00560-x

Hector, C.E., Bretz, C.A., Zhao, Y., and Johnson, E.C. 2009. Functional differences between two CRF-related diuretic hormone receptors in *Drosophila*. *Journal of Experimental Biology* **212**: 3142-3147. DOI: 10.1242/jeb.033175

Hodge, J.J. 2009. Ion channels to inactivate neurons in *Drosophila*. *Frontiers in molecular neuroscience* **13**. DOI: https://doi.org/10.3389/neuro.02.013.2009

Jais, A. and Brüning, J.C. 2022. Arcuate nucleus-dependent regulation of metabolism—pathways to obesity and diabetes mellitus. *Endocrine reviews* **43**: 314-328. DOI: https://doi.org/10.1210/endrev/bnab025

Jia, X., Xu, W., Zhang, L., Li, X., Wang, R., and Wu, S. 2021. Impact of gut microbiota and microbiota-related metabolites on hyperlipidemia. *Frontiers in Cellular and Infection Microbiology* **11**: 634780. DOI: https://doi.org/10.3389/fcimb.2021.634780

Johnson, A.A. and Stolzing, A. 2019. The role of lipid metabolism in aging, lifespan regulation, and age-related disease. *Aging cell* **18**: e13048. DOI: 10.1111/acel.13048

Kim, H.-S., Ren, G., Kim, T., Bhatnagar, S., Yang, Q., Bahk, Y.Y., and Kim, J. 2020. Metformin reduces saturated fatty acid-induced lipid accumulation and inflammatory response by restoration of autophagic flux in endothelial cells. *Scientific reports* **10**: 1-14. DOI: https://doi.org/10.1038/s41598-020-70347-w

Kim, J., Chung, Y.D., Park, D.-y., Choi, S., Shin, D.W., Soh, H., Lee, H.W., Son, W., Yim, J., and Park, C.-S. 2003. A TRPV family ion channel required for hearing in *Drosophila*. *Nature* **424**: 81-84. DOI: 10.1038/nature01733

Kim, J., Yang, G., Kim, Y., Kim, J., and Ha, J. 2016. AMPK activators: mechanisms of action and physiological activities. *Experimental & molecular medicine* **48**: e224-e224. DOI: https://doi.org/10.1038/emm.2016.16

Lee, G.J., Han, G., Yun, H.M., Lim, J.J., Noh, S., Lee, J., and Hyun, S. 2018a. Steroid signaling mediates nutritional regulation of juvenile body growth via IGF-binding protein in *Drosophila*. *Proceedings of the National Academy of Sciences* **115**: 5992-5997. DOI: https://doi.org/10.1073/pnas.1718834115

Lee, J.H., Koh, H., Kim, M., Kim, Y., Lee, S.Y., Karess, R.E., Lee, S.-H., Shong, M., Kim, J.-M., and Kim, J. 2007. Energy-dependent regulation of cell structure by AMP-activated protein kinase. *Nature* **447**: 1017-1020. DOI: 10.1038/nature05828

Lee, Y., Lee, Y., Lee, J., Bang, S., Hyun, S., Kang, J., Hong, S.-T., Bae, E., Kaang, B.-K., and Kim, J. 2005. Pyrexia is a new thermal transient receptor potential channel endowing tolerance to high temperatures in *Drosophila melanogaster*. *Nature genetics* **37**: 305-310. DOI: 10.1038/ng1513

Lee, Y., Poudel, S., Kim, Y., Thakur, D., and Montell, C. 2018b. Calcium taste avoidance in *Drosophila*. *Neuron* **97**: 67-74. e64. DOI: https://doi.org/10.1016/j.neuron.2017.11.038

Liu, T.-T., Liu, X.-T., Chen, Q.-X., and Shi, Y. 2020. Lipase inhibitors for obesity: A review. *Biomedicine & Pharmacotherapy* **128**: 110314. DOI: 10.1016/j.biopha.2020.110314

Liu, Z. and Huang, X. 2013. Lipid metabolism in *Drosophila*: development and disease. *Acta Biochimica et Biophysica Sinica* **45**: 44-50. DOI: 10.1093/abbs/gms105

Lu, K., Zhou, J., Chen, X., Li, W., Li, Y., Cheng, Y., Yan, J., You, K., Yuan, Z., and Zhou, Q. 2018. Deficiency of brummer impaires lipid mobilization and JH-mediated vitellogenesis in the brown planthopper, *Nilaparvata lugens*. *Frontiers in Physiology* **9**: 1535. DOI: 10.3389/fphys.2018.01535

Lv, Z. and Guo, Y. 2020. Metformin and its benefits for various diseases. *Frontiers in endocrinology* **11**: 191. DOI: 10.3389/fendo.2020.00191

Men, T.T., Thanh, D.N.V., Yamaguchi, M., Suzuki, T., Hattori, G., Arii, M., Huy, N.T., and Kamei, K. 2016. A *Drosophila* model for screening antiobesity agents. *BioMed research international* 2016. DOI: 10.1155/2016/6293163

Meunier, N., Belgacem, Y.H., and Martin, J.-R. 2007. Regulation of feeding behaviour and locomotor activity by takeout in *Drosophila*. Journal of Experimental Biology. **210**: 1424-1434. DOI: https://doi.org/10.1242/jeb.02755

Miyamoto, T. and Amrein, H. 2019. Neuronal gluconeogenesis regulates systemic glucose homeostasis in *Drosophila melanogaster*. *Current Biology* **29**: 1263-1272. e1265. DOI: 10.1016/j.cub.2019.02.053

Nath, D.K. and Lee, Y. 2024. Exploring the multifaceted functions of amyloid precursor protein-like (APPL) in metabolism and memory using *Drosophila melanogaster*. *Molecules and Cells* **48**:100163. DOI: https://doi.org/10.1016/j.mocell.2024.100163

Nazario-Yepiz, N.O., Fernández Sobaberas, J., Lyman, R., Campbell III, M.R., Shankar, V., Anholt, R.R., and Mackay, T.F. 2021. Physiological and metabolomic consequences of reduced expression of the *Drosophila* brummer triglyceride Lipase. *PloS one* **16**: e0255198. DOI: https://doi.org/10.1371/journal.pone.0255198

Oh, Y., Lai, J.S.-Y., Min, S., Huang, H.-W., Liberles, S.D., Ryoo, H.D., and Suh, G.S. 2021. Periphery signals generated by Piezo-mediated stomach stretch and Neuromedin-mediated glucose load regulate the *Drosophila* brain nutrient sensor. *Neuron* **109**: 1979-1995. e1976. DOI: https://doi.org/10.1016/j.neuron.2021.04.028

Oh, Y. and Suh, G.S. 2023. Starvation-induced sleep suppression requires the *Drosophila* brain nutrient sensor. *Journal of Neurogenetics* **37**: 70-77. DOI: https://doi.org/10.1080/01677063.2023.2203489

Ohhara, Y., Kobayashi, S., Yamakawa-Kobayashi, K., and Yamanaka, N. 2018. Adult-specific insulin-producing neurons in *Drosophila melanogaster*. *Journal of Comparative Neurology* **526**: 1351-1367. DOI: 10.1002/cne.24410

Overgaard, J., Sørensen, J.G., Petersen, S.O., Loeschcke, V., and Holmstrup, M. 2005. Changes in membrane lipid composition following rapid cold hardening in *Drosophila melanogaster*. *Journal of insect physiology* **51**: 1173-1182. DOI: 10.1016/j.jinsphys.2005.06.007

Picard, M., McEwen, B.S., Epel, E.S., and Sandi, C. 2018. An energetic view of stress: Focus on mitochondria. *Frontiers in neuroendocrinology* **49**: 72-85. DOI: 10.1016/j.yfrne.2018.01.001

Roh, E. and Kim, M.-S. 2016. Brain regulation of energy metabolism. *Endocrinology and metabolism* **31**: 519. DOI: 10.3803/EnM.2016.31.4.519

Sang, J., Dhakal, S., and Lee, Y. 2021. Cucurbitacin B suppresses hyperglycemia associated with a high sugar diet and promotes sleep in Drosophila melanogaster. *Molecules and cells* **44**: 68-78. DOI: 10.14348/molcells.2021.2245

Szkudelski, T., Konieczna, K., and Szkudelska, K. 2022. Regulatory Effects of Metformin, an Antidiabetic Biguanide Drug, on the Metabolism of Primary Rat Adipocytes. *Molecules* **27**: 5250. DOI: 10.3390/molecules27165250

Tatar, M., Post, S., and Yu, K. 2014. Nutrient control of *Drosophila* longevity. *Trends in Endocrinology & Metabolism* **25**: 509-517. DOI: 10.1016/j.tem.2014.02.006

Tracey Jr, W.D., Wilson, R.I., Laurent, G., and Benzer, S. 2003. painless, a *Drosophila* gene essential for nociception. *Cell* **113**: 261-273. DOI: 10.1016/s0092-8674(03)00272-1

Tran, L.T., Park, S., Kim, S.K., Lee, J.S., Kim, K.W., and Kwon, O. 2022. Hypothalamic control of energy expenditure and thermogenesis. *Experimental & Molecular Medicine* **54**: 358-369. DOI: https://doi.org/10.1038/s12276-022-00741-z

Turner, H.N., Armengol, K., Patel, A.A., Himmel, N.J., Sullivan, L., Iyer, S.C., Bhattacharya, S., Iyer, E.P.R., Landry, C., and Galko, M.J. 2016. The TRP channels Pkd2, NompC, and Trpm act in cold-sensing neurons to mediate unique aversive behaviors to noxious cold in *Drosophila*. *Current biology* **26**: 3116-3128. DOI: 10.1016/j.cub.2016.09.038

Venkatachalam, K. and Montell, C. 2007. TRP channels. Annual Review of Biochemistry. **76**: 387-417. DOI: 10.1146/annurev.biochem.75.103004.142819

Wang, Y., Yu, W., Li, S., Guo, D., He, J., and Wang, Y. 2022. Acetyl-CoA carboxylases and diseases. *Frontiers in Oncology* **12**: 836058. DOI: https://doi.org/10.3389/fonc.2022.836058

Watnick, T.J., Jin, Y., Matunis, E., Kernan, M.J., and Montell, C. 2003. A flagellar polycystin-2 homolog required for male fertility in *Drosophila*. *Current Biology* **13**: 2179-2184. DOI: 10.1016/j.cub.2003.12.002

Yee, J.K., Wahjudi, P.N., Vega, J., Lim, S., Martin, A., Patterson, M.E., Cohen, J.N., Mao, C.S., and Lee, W.-N.P. 2013. Stearoyl-CoA desaturase enzyme 1 inhibition reduces glucose utilization for de novo fatty acid synthesis and cell proliferation in 3T3-L1 adipocytes. *Metabolomics* **9**: 809-816. DOI: 10.1007/s11306-013-0511-3

Yoshinari, Y., Kosakamoto, H., Kamiyama, T., Hoshino, R., Matsuoka, R., Kondo, S., Tanimoto, H., Nakamura, A., Obata, F., and Niwa, R. 2021. The sugar-responsive enteroendocrine neuropeptide F regulates lipid metabolism through glucagon-like and insulin-like hormones in *Drosophila melanogaster*. *Nature communications* **12**: 4818. DOI: https://doi.org/10.1038/s41467-021-25146-w

Figure Legends

Figure 1. TRPγ mutants exhibit altered carbohydrate, lipid, and protein levels. (**A**) TAG level measurement in the whole-body extract from control (w^{1118}) and TRP channel mutant lines (n=9). (**B**) Protein level measurement in the whole-body extract from control (w^{1118}) and TRP channel mutant lines (n=6). (**C**) Measurement of total glucose and trehalose levels (µg/mg) in the whole-body extracts of control (w^{1118}) and $trp\gamma^{1}$ adult males (n=6). (**D**) Measurement of tissue glycogen levels (µg/mg) in adult control (w^{1118}) and $trp\gamma^{1}$ males (n=6). (**E**) Measurement of Hemolymph glucose + trehalose level in the male flies of control (w^{1118}) and $trp\gamma^{1}$ (n=6). (**F**) Measurement of TAG level in adult males to test for rescue of the TAG defect in *trpγ* flies with the *UAS-trpγ* and the $trp\gamma^{G4}$ or with the *trpγ* genomic transgene (n=6-10). (**G**) Rescue experiments showing the measurement of protein levels in adult flies with the indicated genotypes (n=6). Comparisons between multiple experimental groups were conducted via single-factor ANOVA coupled with Scheffe's *post hoc* test. The asterisks indicate significant differences from the controls (**P<0.01).

Figure 2. *Dh44* neurons are essential for regulating lipid tissue levels. (**A**) Tissue TAG level measurement in whole-body extracts of adult male flies after silencing of *Dh44-GAL4* and *dILP2-GAL4* with *UAS-Kir2.1* (n=6). (**B**) Measurement of tissue protein level in whole-body extracts of adult male flies. Brain-specific *Dh44-GAL4* and *dILP2-GAL4* neurons were ablated using *UAS-Kir2.1* (n=6). (**C**) Measurement of TAG from whole-body extract of adult male flies in the indicated genotypes (n=6-7). (**D**) Measurement of

tissue protein level from the whole-body extracts of adult males (n=6). (**E**) TAG levels in whole-body extracts after RNAi knockdown of *trpγ* mutants under control of the *Dh44-GAL4* (n=6). (**F**) Measurement of area (μm^2) of LDs in adult fat body across the indicated genotypes involved the selection of the 30 largest LDs, choosing the top 10 LDs from each sample for analysis (n=3). (**G**–**L**) Nile red stating of fat body from the male of indicated genotypes. The scale bar represents 50 μm.

All values are reported as means ± SEM. Comparisons between multiple experimental groups were conducted via single-factor ANOVA coupled with Scheffe's *post hoc* test. The asterisks indicate significant differences from the controls (**P*<0.05, ***P*<0.01). Each dot indicates the distribution of individual sample values. (+) and (-) indicate the presence or absence of the indicated transgenes, respectively.

Figure 3. *trpγ^1* have deficits in the lipolytic pathway under starvation conditions. (**A**) Survival assay to measure the total survival time (days) of control (*w^{1118}*) and *trpγ^1* male flies fed with a normal corn meal diet (n=7-8). (**B**) Survival assay to measure the survival time (h) of the indicated genotypes with male flies under starvation conditions (n=4). (**C**) TAG level measurement in control (*w^{1118}*) and *trpγ^1* adult male flies in both sated (0 h starvation) and starved (24 h starvation) conditions (n=8). (**D**–**E**) Nile red staining of the LDs extracted from FB of (D) *w^{1118}* and (E) *trpγ^1* flies under sated (**D1** and **E1**) and starved (**D2** and **E2**) conditions, respectively. The scale bar represents 50 μm. (**F**) Measurement of area (μm^2) of the LDs extracted from the FBs of *w^{1118}* and *trpγ^1* flies under sated (0 h starvation) and starved (24 h starvation) conditions (n=3). (**G**)

Measurement of TAG level with controls and the flies after expressing *UAS-AMPK*^{TD} under the control of *Dh44-GAL4* in the *trp*γ^{1} mutant background (n=4).

All values are reported as means ± SEM. Survival curves in A and B were estimated for each group, using a Kaplan-Meier method and compared statistically using the log-rank tests. Comparisons between multiple experimental groups in C, F, G, and H were conducted via single-factor ANOVA coupled with Scheffe's *post hoc* test. The asterisks indicate significant differences from the controls (**P<0.01).

Figure 4. Rescue of starvation susceptibility phenotype using the lipolytic drug metformin**.** (**A**) TAG level measurement at 0, 7, and 14 days in the control (w^{1118}) and *trp*γ^{1} adult male flies after dietary exposure to 1 mM metformin (n=6). (**B**) TAG measurement at 0, 7, and 14 days in w^{1118} and *trp*γ^{1} adult male flies after dietary exposure to 5 mM metformin (n=6). (**C**) Pictures of Nile red staining of LDs after dietary exposure to 1 mM and 5 mM metformin in standard fly food for 7 and 14 days in w^{1118} and *trp*γ^{1} flies. The scale bars represent 50 µm. (**D**) Measurement of area (µm^2) of LDs extracted from the FB of w^{1118} and *trp*γ^{1} flies after dietary exposure to 1mM and 5 mM metformin in standard fly food for 7 and 14 days (n=3). (**E**) Survival assay to measure the survival time (h) of control (w^{1118}) and *trp*γ^{1} males after dietary exposure to 1 mM metformin in 1% agar food (n=6-10). (**F**) Starvation survival assay of control (w^{1118}) and *trp*γ^{1} males after dietary exposure to 5 mM metformin in 1% agar food (n=6).

All values are reported as means ± SEM. Comparisons between multiple experimental groups were conducted via single-factor ANOVA coupled with Scheffe's *post hoc* test.

Each dot indicates the distribution of individual sample values. Survival curves in E and F were estimated for each group, using a Kaplan-Meier method and compared statistically using the log-rank tests. The asterisks indicate significant differences from the controls (**P<0.01).

Figure 5. Quantitative analysis of the expression of gluconeogenic, lipogenic, and lipolytic genes and the effect of *bmm* expression and metformin feeding. (**A**) qRT-PCR analysis to measure the expression of gluconeogenic genes (*fbp*, *pepck1*), lipogenic genes (*acc*, *desat1*), and a lipolytic gene (*bmm*) under sated (0 h starvation) and starved (24 h starvation) conditions in w^{1118} and $trp\gamma^{1}$ flies. The relative fold change in the expression of starvation-induced genes (gluconeogenic genes: *fbp* and *pepck1*; lipogenic genes: *acc* and *desat1;* and lipolytic gene: *bmm*) was determined in whole-body samples of male adult w^{1118} and $trp\gamma^{1}$ flies by qRT-PCR. *Tubulin* was used as an internal control to standardize the samples. Each graph shows the number of evaluated samples (n=3). (**B**) Fluorescence microscopic imaging of *bmm*::*GFP* expression in the FBs of w^{1118} and $trp\gamma^{1}$ under sated (0 h starvation) and starvation (24 h starvation) conditions. The scale bar represent 50 µm. (**C**) Quantification of intensity level of *bmm*::*GFP* in the FBs of w^{1118} and $trp\gamma^{1}$ under sated and starvation conditions (n=3). (**D**–**I**) Nile red staining of lipids in the FB of flies with the indicated genotypes. The scale bar represent 50 µm. (**J**) Measurement of area of LDs from samples D–I entailed selecting a total of 30 LDs, with the 10 largest LDs chosen from each sample for analysis (n=3). (**K**) qRT-PCR analysis to measure the expression of *acc*, *desat1*, and *bmm* from the whole body samples of flies after feeding 5 mM metformin for 1 day (n=3).

All values are reported as means ± SEM. Comparisons between multiple experimental groups were conducted via single-factor ANOVA coupled with Scheffe's *post hoc* test. The asterisks indicate significant differences from the controls (*P<0.05, **P<0.01).

Figure 6. Dietary supply of lipase, glycerol, mixed TAG, and free FA to rescue the starvation sensitivity phenotype. (**A**) Survival assays of w^{1118} and $trp\gamma^{1}$ flies under starvation condition by feeding 0.1% lipase or 0.1% denatured lipase mixed into 1% agar food (n=8). (**B**) Starvation survival assay to measure the survival time (h) of w^{1118} and $trp\gamma^{1}$ male flies after feeding 1% glycerol mixed into 1% agar food (n=4). (**C**) Survival assay to measure the survival time (h) of w^{1118} and $trp\gamma^{1}$ flies after feeding 0.2% hexanoic acid (HA) supplemented into 1% agar food (n=8). (**D**) Survival assay to measure the survival time (h) of w^{1118} and $trp\gamma^{1}$ flies after feeding 0.2% mixed (mono-, di-, and tri-) glycerides (n=4). (**E**–**I**) Nile red staining of LDs in full gut and the magnified R2 region of adult male flies. (**E**) w^{1118}, (**F**) $trp\gamma^{1}$, (**G**) $trp\gamma^{1}$,*UAS-trpγ*/$trp\gamma^{G4}$, (**H**) $trp\gamma^{1}$,*UAS-trpγ*/$trp\gamma^{1}$;*Dh44-GAL4*/+. The scale bar represents 50 µm. The arrow indicates the orientation of intestine from anterior to posterior. (**I**) Measurement of area of LDs in the R2 region of $trp\gamma^{1}$, area of 28 LDs from 10 samples (n=10). Note that control and rescued flies have no LD.

All values are reported as means ± SEM. Survival curves were estimated for each group, using a Kaplan-Meier method and compared statistically using the log-rank tests. (**P<0.01).

Figure 7. Functional analysis of *Dh44*, *Dh44R1*, and *Dh44R2* mutants and their roles in lipid accumulation. (**A**) Total TAG level (µg TAG/mg fly) measurement in whole body extracts from control (w^{1118}), $Dh44^{Mi}$, $Dh44R1^{Mi}$, and $Dh44R2^{Mi}$ mutants (n=5). (**B**–**E**) Nile red stains of the fat body from w^{1118}, $Dh44^{Mi}$, $Dh44R1^{Mi}$, and $Dh44R2^{Mi}$ respectively. Scale bars represent 50 µm. (**F**) Area of LDs in each indicated genotype (n=3). (**G**) The protein (µg protein/mg fly) measurement in the whole-body extracts from control (w^{1118}) and $Dh44^{Mi}$, $Dh44R1^{Mi}$, and $Dh44R2^{Mi}$ mutants (n=4). (**H**) Quantification (qRT-PCR) of lipolytic gene (bmm) expression level in the fat body of w^{1118}, $Dh44^{Mi}$, $Dh44R1^{Mi}$, and $D44R2^{Mi}$ flies under sated and starved conditions (n=3). (**I**) Total TAG level measurement in whole body extracts from the indicated genotypes (n=4). (**J**–**M**) Nile red stains of the fat body from (**J**) w^{1118}, (**K**) $trp\gamma^{1}$ (**L**) $trp\gamma^{1}$,*UAS-*$trp\gamma^{1}$/$trp\gamma^{1}$,*Dh44R1-GAL4*, and (**M**) $trp\gamma^{1}$,*UAS-*$trp\gamma^{1}$/$trp\gamma^{1}$,*Dh44R2-GAL4*. (**N**) Area of LDs in each indicated genotype (n=3). Scale bar represent 50 µm. (**O**–**Q**) Immunohistochemistry with anti-GFP and anti-DsRed. (**O** and **P**) Co-expression of *trpγ* and *Dh44R2* ($trp\gamma^{G4}$/Dh44R2-*LexA*;*UAS-mCD8*::*GFP*/*LexAopmCherry*) in the R2 region of the inetestine. Arrows indicate co-expression of *trpγ* and *Dh44R2* in the gut cell. (**O**) Full gut image. Scale bar represents 300 µm. (**P**) Magnified view of boxed R2 region in **O**. Scale bar represent 50 µm. (**Q**) Co-expression of *Dh44R2* and *Dh44* (*Dh44R2-GAL4*/*Dh44-LexA*;*UAS-mCD8*::*GFP*/*LexAop-mCherry*) in the brain. Arrows indicate coexpressed two cells in the PI. Scale bars represent 50 µm.

Means ±SEMs. Single factor ANOVA with Scheffe's analysis was used as a post hoc test to compare multiple sets of data. The asterisks indicate significance from control (*P < 0.05, **P < 0.01). Each dot indicates distribution of individual sample value.

Figure 8. Schamatic model representing the roles of *trp*γ in metabolic regualtion of carbohydrate, lipid, and protein.

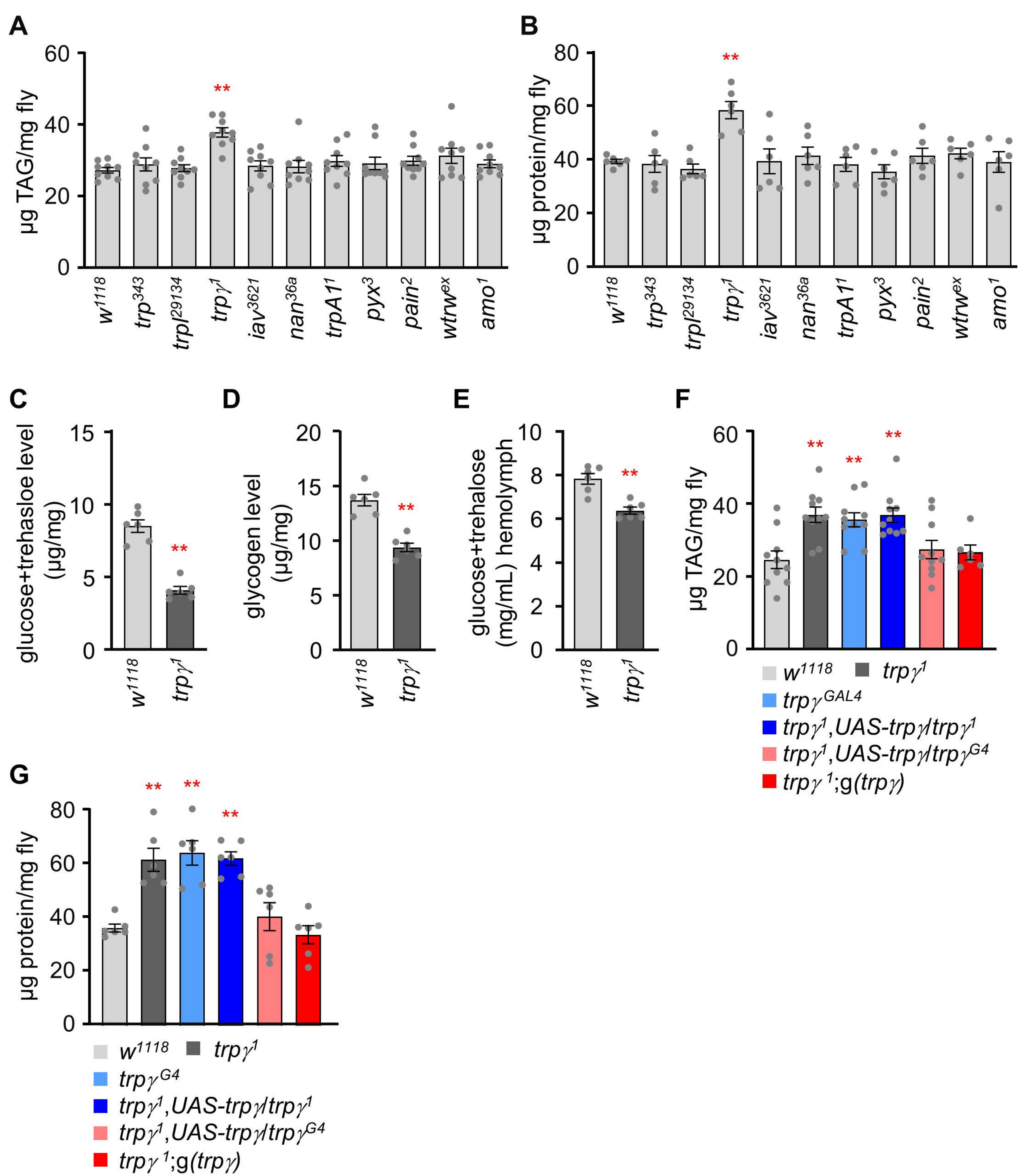
A
µg TAG/mg fly
60
40
20
0
**
w1118
trp343
trpl29134
trpγ1
iav3621
nan36a
trpA11
pyx3
pain2
wtrwex
amo1
B
µg protein/mg fly
80
60
40
20
0
**
C
glucose+trehasloe level (µg/mg)
15
10
5
0
D
glycogen level (µg/mg)
20
15
10
5
E
glucose+trehalose (mg/mL) hemolymph
10
8
6
4
2
F
µg TAG/mg fly
w1118
trpγ1
trpγGAL4
trpγ1,UAS-trpγ/trpγ1
trpγ1,UAS-trpγ/trpγG4
trpγ 1;g(trpγ)
G
µg protein/mg fly

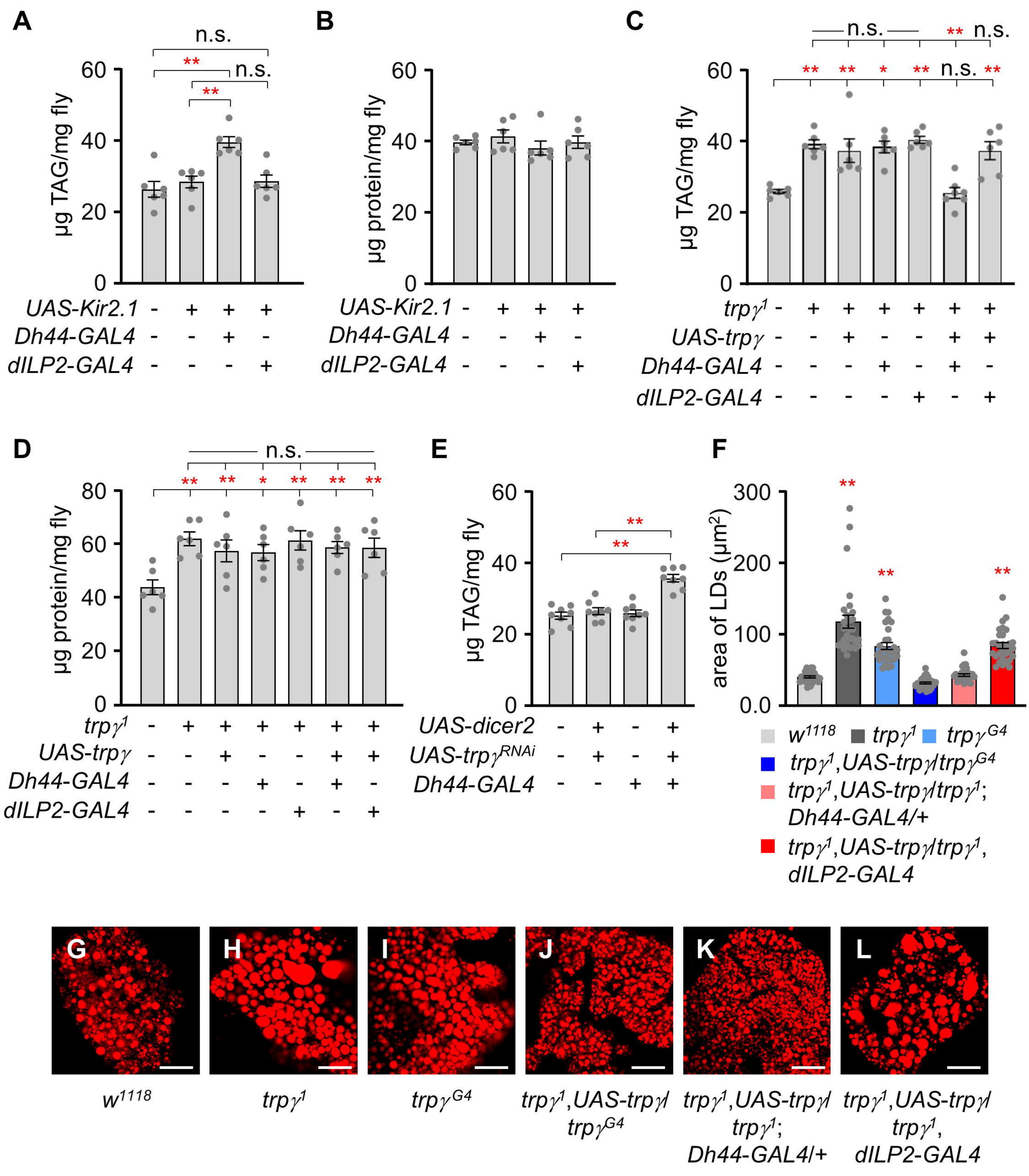
A
n.s.
**
n.s.
**
µg TAG/mg fly
60
40
20
0
UAS-Kir2.1 - + + +
Dh44-GAL4 - - + -
dILP2-GAL4 - - - +
B
µg protein/mg fly
60
40
20
0
UAS-Kir2.1 - + + +
Dh44-GAL4 - - + -
dILP2-GAL4 - - - +
C
n.s.
** n.s.
** ** * ** n.s. **
µg TAG/mg fly
60
40
20
0
trpγ1 - + + + + + +
UAS-trpγ - - + - - + +
Dh44-GAL4 - - - + - + -
dILP2-GAL4 - - - - + - +
D
n.s.
** ** * ** ** **
µg protein/mg fly
80
60
40
20
0
trpγ1 - + + + + + +
UAS-trpγ - - + - - + +
Dh44-GAL4 - - - + - + -
dILP2-GAL4 - - - - + - +
E
**
**
µg TAG/mg fly
60
40
20
0
UAS-dicer2 - + - +
UAS-trpγRNAi - + - +
Dh44-GAL4 - - + +
F
**
**
**
area of LDs (µm2)
300
200
100
0.0
w1118
trpγ1
trpγG4
trpγ1,UAS-trpγ/trpγG4
trpγ1,UAS-trpγ/trpγ1; Dh44-GAL4/+
trpγ1,UAS-trpγ/trpγ1, dILP2-GAL4
G
H
I
J
K
L
w1118
trpγ1
trpγG4
trpγ1,UAS-trpγ/ trpγG4
trpγ1,UAS-trpγ/ trpγ1; Dh44-GAL4/+
trpγ1,UAS-trpγ/ trpγ1, dILP2-GAL4

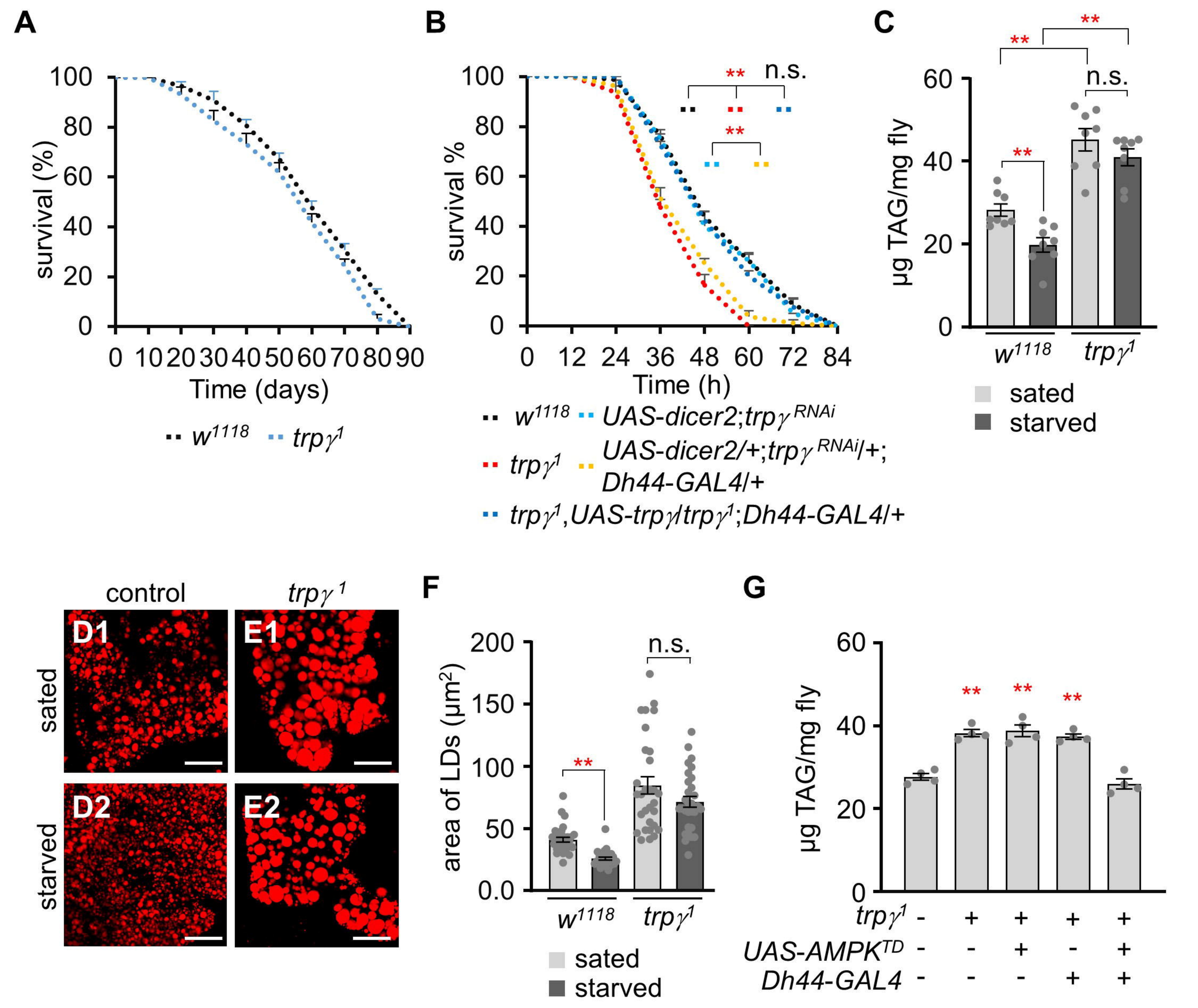
A
survival (%)
Time (days)
w1118
trpγ1
B
survival %
Time (h)
**
n.s.
w1118
UAS-dicer2;trpγRNAi
trpγ1
UAS-dicer2/+;trpγRNAi/+;
Dh44-GAL4/+
trpγ1,UAS-trpγ/trpγ1;Dh44-GAL4/+
C
µg TAG/mg fly
w1118
trpγ1
sated
starved
control
trpγ1
sated
starved
D1
E1
D2
E2
F
area of LDs (µm2)
n.s.
w1118
trpγ1
sated
starved
G
µg TAG/mg fly
trpγ1
UAS-AMPKTD
Dh44-GAL4

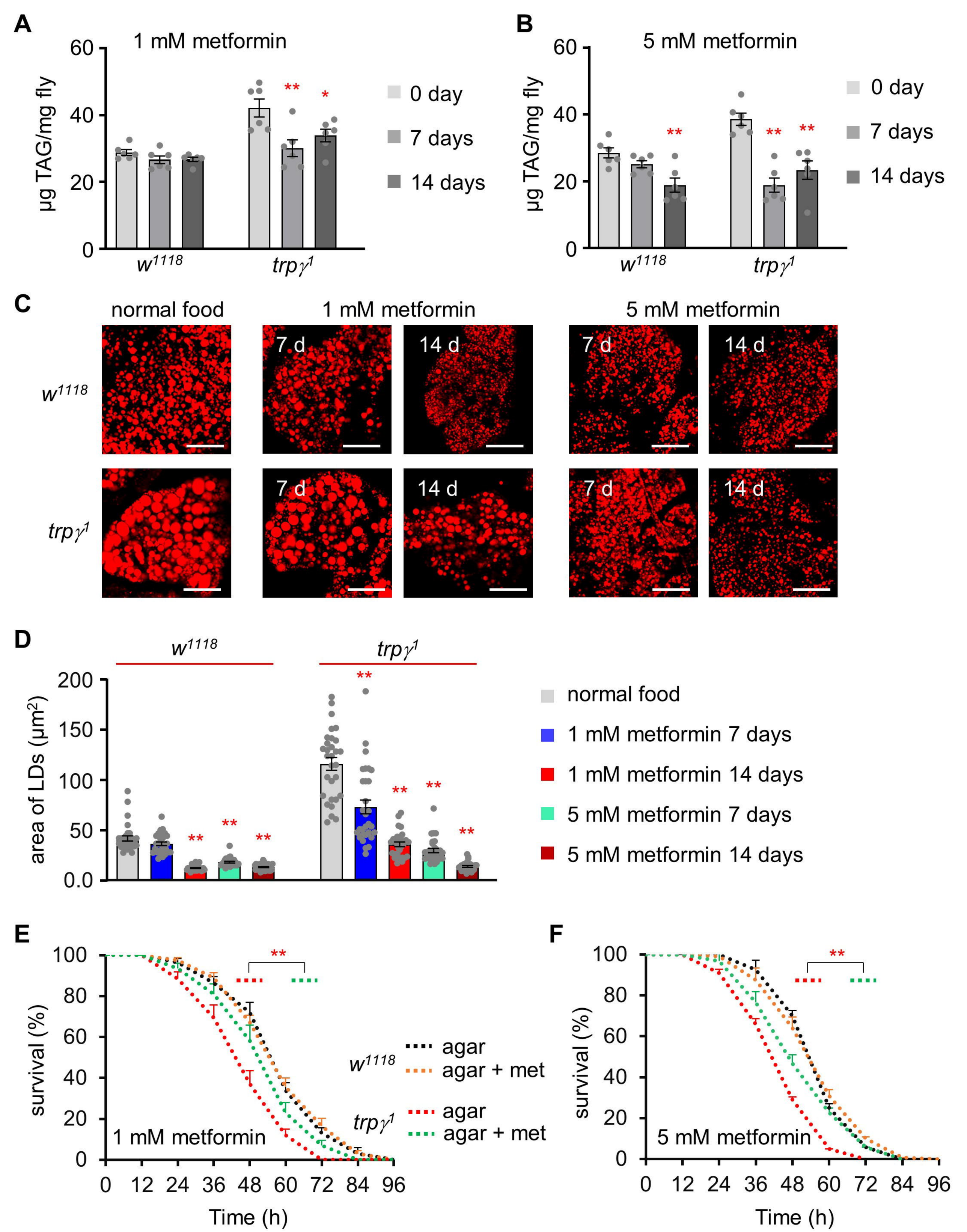
A
1 mM metformin
μg TAG/mg fly
60
40
20
0
**
*
0 day
7 days
14 days
w1118
trpγ1
B
5 mM metformin
μg TAG/mg fly
60
40
20
0
**
**
**
0 day
7 days
14 days
w1118
trpγ1
C
normal food
1 mM metformin
5 mM metformin
w1118
trpγ1
7 d
14 d
7 d
14 d
7 d
14 d
7 d
14 d
D
w1118
trpγ1
area of LDs (μm2)
200
150
100
50
0.0
**
**
**
**
**
**
**
normal food
1 mM metformin 7 days
1 mM metformin 14 days
5 mM metformin 7 days
5 mM metformin 14 days
E
survival (%)
100
80
60
40
20
0
**
1 mM metformin
w1118
trpγ1
agar
agar + met
agar
agar + met
0 12 24 36 48 60 72 84 96
Time (h)
F
survival (%)
100
80
60
40
20
0
**
5 mM metformin
0 12 24 36 48 60 72 84 96
Time (h)

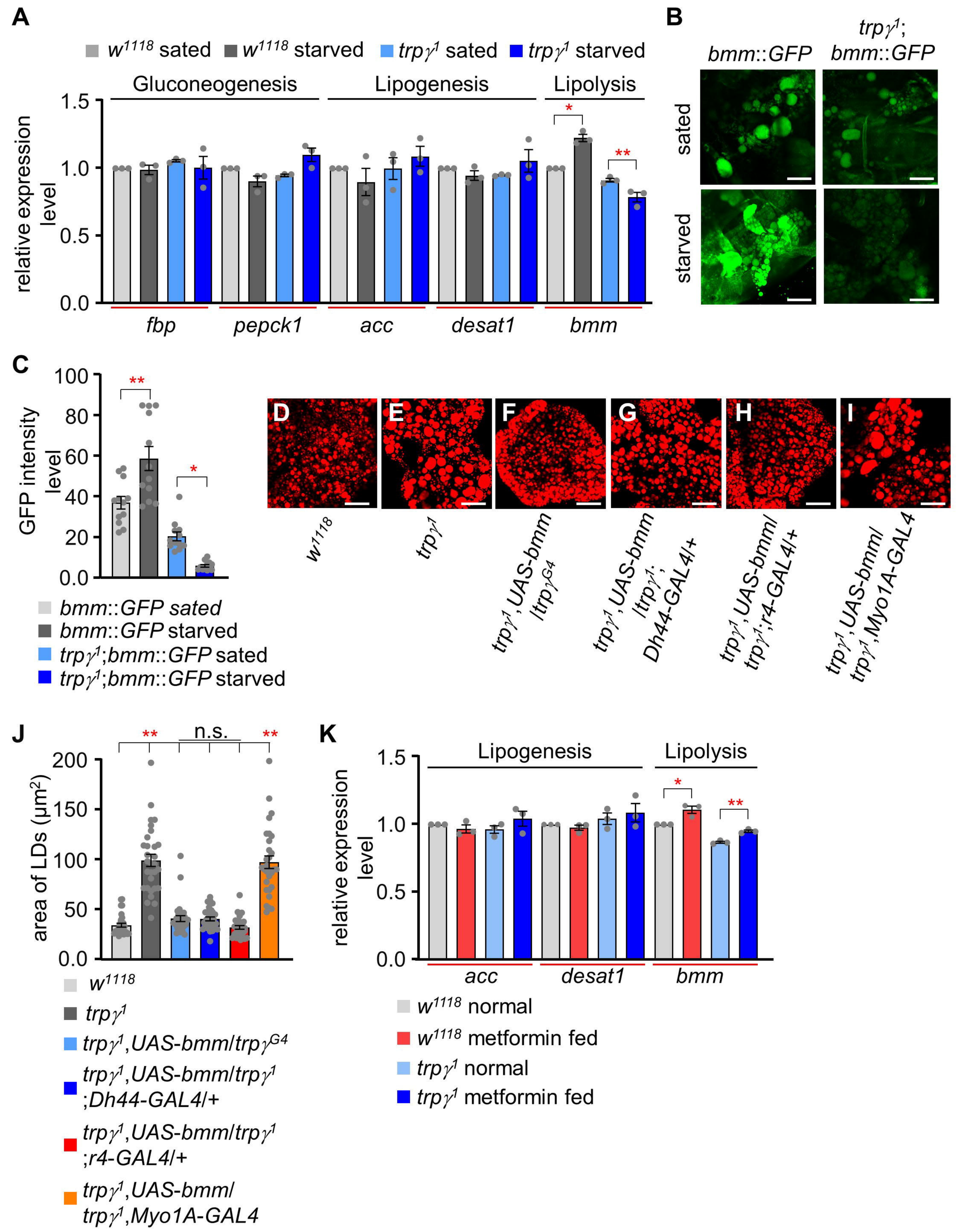
A
w1118 sated
w1118 starved
trpγ1 sated
trpγ1 starved
Gluconeogenesis
Lipogenesis
Lipolysis
relative expression level
1.5
1.0
0.5
0.0
*
**
fbp
pepck1
acc
desat1
bmm
B
bmm::GFP
trpγ1; bmm::GFP
sated
starved
C
GFP intensity level
100
80
60
40
20
0.0
**
*
bmm::GFP sated
bmm::GFP starved
trpγ1;bmm::GFP sated
trpγ1;bmm::GFP starved
D
E
F
G
H
I
w1118
trpγ1
trpγ1,UAS-bmm /trpγG4
trpγ1,UAS-bmm /trpγ1; Dh44-GAL4/+
trpγ1,UAS-bmm/ trpγ1;r4-GAL4/+
trpγ1,UAS-bmm/ trpγ1,Myo1A-GAL4
J
area of LDs (μm2)
200
150
100
50
0.0
**
n.s.
**
w1118
trpγ1
trpγ1,UAS-bmm/trpγG4
trpγ1,UAS-bmm/trpγ1 ;Dh44-GAL4/+
trpγ1,UAS-bmm/trpγ1 ;r4-GAL4/+
trpγ1,UAS-bmm/ trpγ1,Myo1A-GAL4
K
relative expression level
1.5
1.0
0.5
0.0
Lipogenesis
Lipolysis
*
**
acc
desat1
bmm
w1118 normal
w1118 metformin fed
trpγ1 normal
trpγ1 metformin fed

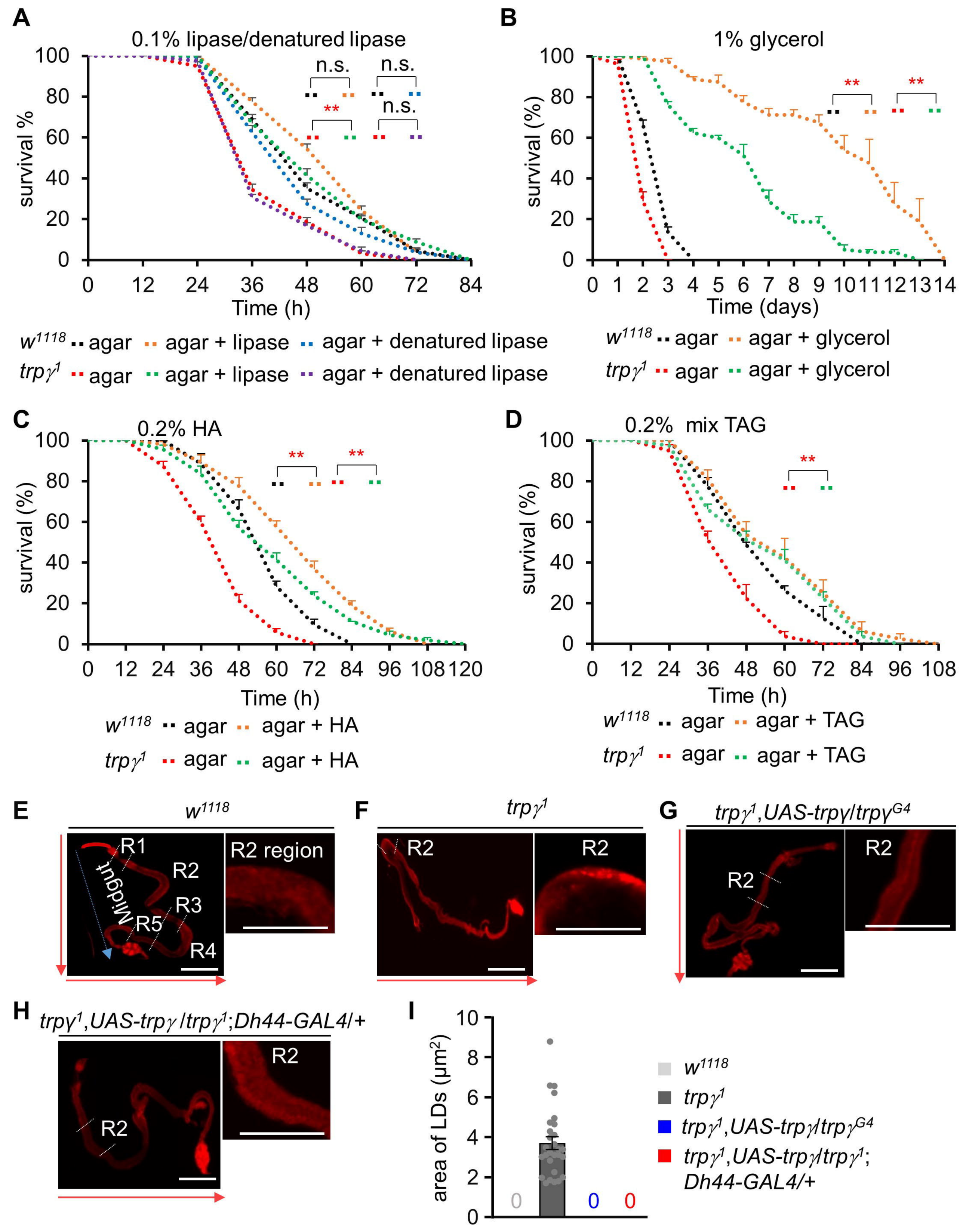
A
0.1% lipase/denatured lipase
survival %
Time (h)
n.s.
n.s.
**
n.s.
w1118 agar agar + lipase agar + denatured lipase
trpγ1 agar agar + lipase agar + denatured lipase
B
1% glycerol
survival (%)
Time (days)
**
**
w1118 agar agar + glycerol
trpγ1 agar agar + glycerol
C
0.2% HA
survival (%)
Time (h)
**
**
w1118 agar agar + HA
trpγ1 agar agar + HA
D
0.2% mix TAG
survival (%)
Time (h)
**
w1118 agar agar + TAG
trpγ1 agar agar + TAG
E
w1118
R1
R2
R3
R4
R5
Midgut
R2 region
F
trpγ1
R2
R2
G
trpγ1,UAS-trpγ/trpγG4
R2
R2
H
trpγ1,UAS-trpγ/trpγ1;Dh44-GAL4/+
R2
R2
I
area of LDs (μm2)
0
0
0
w1118
trpγ1
trpγ1,UAS-trpγ/trpγG4
trpγ1,UAS-trpγ/trpγ1;
Dh44-GAL4/+

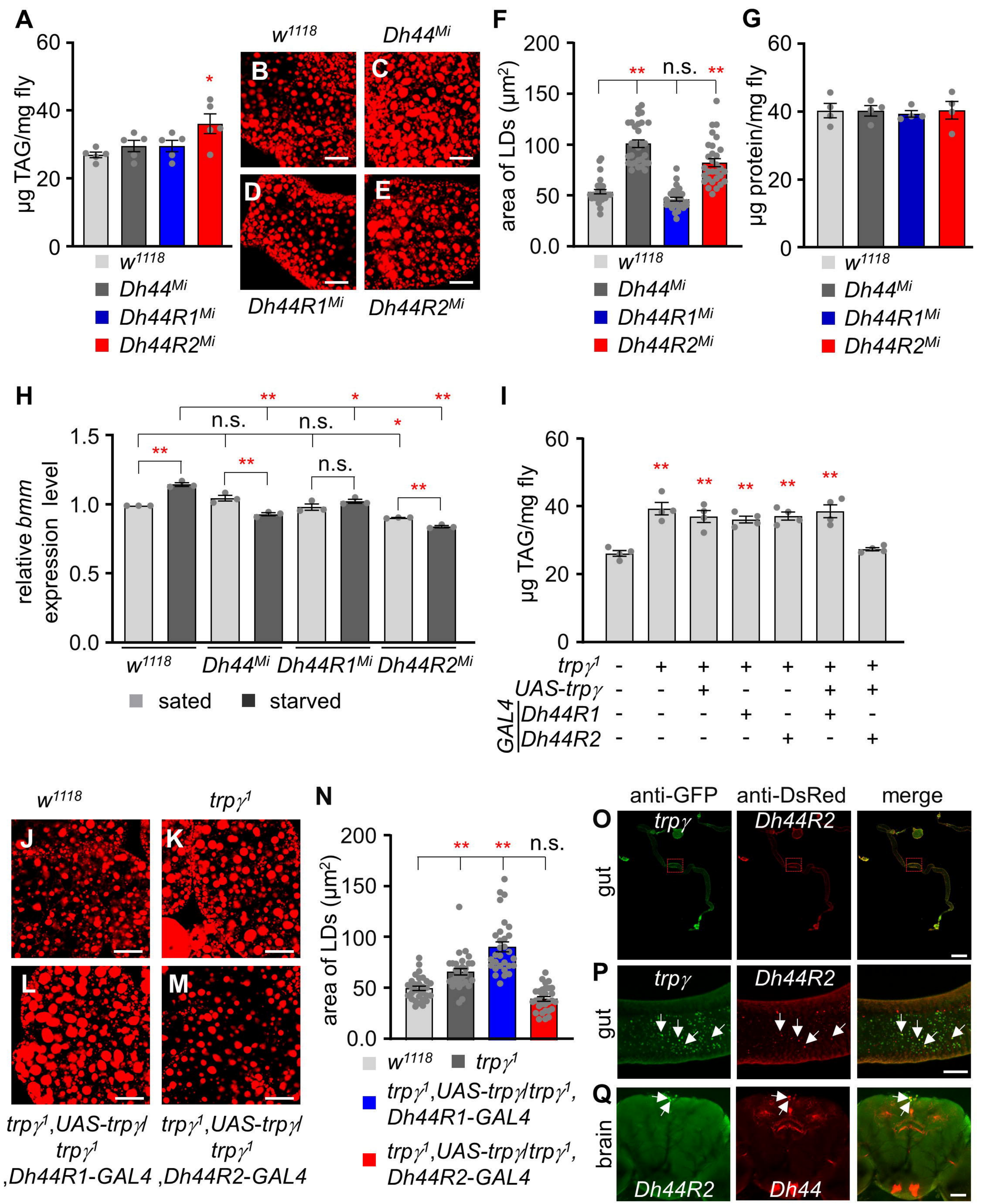
A
μg TAG/mg fly
w1118
Dh44Mi
Dh44R1Mi
Dh44R2Mi
B
C
D
E
F
area of LDs (μm2)
n.s.
G
μg protein/mg fly
H
relative bmm expression level
sated
starved
I
μg TAG/mg fly
trpγ1
UAS-trpγ
GAL4
Dh44R1
Dh44R2
J
K
L
M
trpγ1,UAS-trpγ/trpγ1,Dh44R1-GAL4
trpγ1,UAS-trpγ/trpγ1,Dh44R2-GAL4
N
area of LDs (μm2)
trpγ1,UAS-trpγ/trpγ1, Dh44R1-GAL4
trpγ1,UAS-trpγ/trpγ1, Dh44R2-GAL4
anti-GFP
anti-DsRed
merge
O
P
Q
gut
brain
trpγ
Dh44R2
Dh44

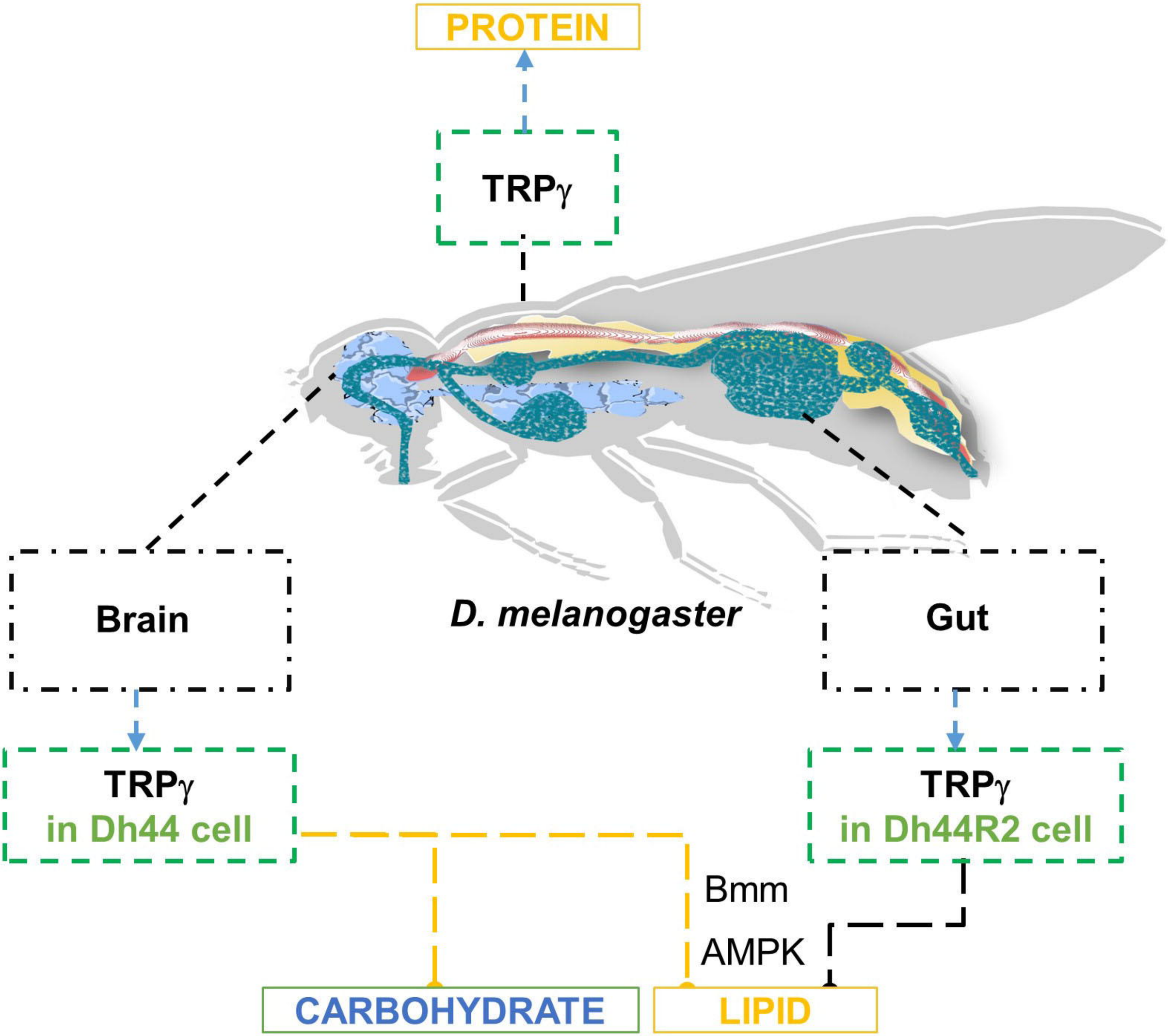
PROTEIN
TRPγ
Brain
D. melanogaster
Gut
TRPγ
in Dh44 cell
TRPγ
in Dh44R2 cell
Bmm
AMPK
CARBOHYDRATE
LIPID